



First-principles-only CALPHAD phase diagram of the solid aluminium-nickel (Al-Ni) system

Theresa Davey^{*}, Nguyen-Dung Tran, Arkapol Saengdeejeing, Ying Chen

School of Engineering, Tohoku University, Sendai, 980-8579, Japan

ARTICLE INFO

Keywords:

Aluminum
Nickel
Phase diagram
First-principles
CALPHAD
Order-disorder model

ABSTRACT

Phase diagrams obtained from first-principles have the potential to reduce time and expense by guiding experimental investigations for materials design applications. However, simply substituting all experimental data with calculated single phase quantities alone has generally shown limited success in the standard CALPHAD modelling of binary or multicomponent systems. In this work, the solid aluminium-nickel system is described using Bragg-Williams-Gorsky approximations in combination with order-disorder partitioning models, where all parameters are obtained directly from first-principles calculation without optimisation considering any phase diagram data. The resulting phase diagram reproduces all major features of the experimentally known phase diagram at a practical application level. This work demonstrates that by careful consideration of the Gibbs energy models and the accuracy of the first-principles calculation, it is possible to obtain a first-principles CALPHAD-type thermodynamic description without conventional optimisation based on experimental data.

1. Introduction

Experimental investigations for thermodynamics-based phase diagram studies are time-consuming and expensive, and many important techniques that are key for determining certain material properties, such as calorimetry, have begun to fade into obscurity as experimental setups become few and far between. The time, money, and skillsets needed to conduct thorough phase diagram investigations experimentally rarely exist in a modern academic climate, and as such, evaluations of phase diagrams are usually conducted using experimental data that is many decades old. In terms of experimental data, it is certainly not a truism that old is necessarily bad and new is necessarily good, however, improved experimental technologies have enhanced our knowledge of impurity levels, reduced uncertainties in measurement, and allowed measurement of properties that were previously not possible to consider, all of which are important for phase diagram evaluations. Furthermore, modern literature has the advantage of usually having a far more consistent standard of documentation, which is unfortunately often untrue of older studies, and consequently evaluating experimental data for a careful phase diagram assessment takes significant time belabouring each and every data point.

By contrast, in recent decades first-principles calculations have

continued to improve, with certain calculations being possible with the same, or smaller uncertainty than experimental measurements of the same property [1], and methods being continually improved and validated. Such calculations are important for various databasing efforts such as the Materials Genome Initiative [2], which allow the combination of high-throughput calculations and materials informatics approaches to design potential new materials at the prediction stage.

Although calculations at the forefront of our abilities, for instance temperature dependent thermodynamic properties including even anharmonic vibrational contributions [3], are still time-consuming and computationally expensive, such calculations are becoming more and more tractable every day [4]. First-principles calculations have shown some success in predicting phase diagrams for simple systems for many years, using a variety of techniques [5]. However, the use of first-principles calculations in thermodynamics-based descriptions that can be easily extended to describe multicomponent systems, as in the CALPHAD approach, has been mostly limited to enhancing descriptions alongside experimental data. Where first-principles calculations have been used without experimental data, the results have often failed to reproduce physical features, which may be attributed to the wealth of approximations used in approaches usually applied using experimental data [6].

^{*} Corresponding author.

E-mail addresses: theresa@tohoku.ac.jp (T. Davey), tran.nguyen.dung@rift.mech.tohoku.ac.jp (N.-D. Tran), aksaengdeejeing@rift.mech.tohoku.ac.jp (A. Saengdeejeing), ying@rift.mech.tohoku.ac.jp (Y. Chen).

<https://doi.org/10.1016/j.calphad.2020.102008>

Received 2 June 2020; Received in revised form 3 August 2020; Accepted 9 August 2020

Available online 10 September 2020

0364-5916/© 2020 Elsevier Ltd. All rights reserved.

In this paper, the aluminium-nickel system is used as an example to demonstrate that by making full use of available calculation and thermodynamic modelling techniques, is it possible to produce a physically meaningful and highly quantitative thermodynamic description of a fairly complex solid system using only first-principles calculations of thermodynamic quantities as data. Aluminium-nickel was chosen as the prototype system as it has been very extensively studied and displays several common phase diagram features that can be challenging to model. These include a variety of invariant reactions, order-disorder transitions, and varying degrees of solubility. It is shown that with a CALPHAD-type description populated with only first-principles data, it is possible to correctly predict phase boundaries and ordering behaviour for a variety of solid-based phases of different structure types.

2. The Al-Ni system

Many versions of the experimental and calculated phase diagram of the aluminium-nickel system are available. It is generally accepted that the following condensed phases are present:

- Liquid
- γ -Al (disordered face-centred cubic (fcc) A1), γ -Ni (fcc A1) at the Al- and Ni-rich ends.
- γ' -AlNi₃ (ordered fcc L1₂ phase) with a narrow range of solubility both above and below stoichiometry
- AlNi (ordered body-centred cubic (bcc) B2 phase) with a wide homogeneity region in both the Al-rich and Ni-rich range
- Al₃Ni₂ (D5₁₃ hexagonal ordered phase) with a narrow range of stability, mostly on the Al-rich side
- Al₃Ni (D0₁₁) stable as a line compound
- Al₃Ni₅ (often labelled with Pearson symbol oC16 or oS16), stable with limited solubility

The Al₄Ni₃ phase has also been reported in several studies [7,8] although it has not been included in most experimental and CALPHAD phase diagrams. In this work, all of the above solid phases were considered, including Al₄Ni₃. The stoichiometric composition, Strukturbericht, Pearson symbol, space group, and prototypes for each phase are given in Table 1.

Of the many CALPHAD-type assessments made of this system, the most commonly used are based on the assessment of Al-Ni by Ansara et al. [9] which models the order-disorder transformation in the fcc phases with either two or four sublattices. Dupin et al. [10] made revisions to this model to adjust the ordering in the fcc and bcc phases. The assessment from Dupin et al. is shown alongside experimental data upon which it is based in Fig. 1.

The aluminium-nickel system has also been very widely studied from a theoretical perspective. Recent first-principles investigations from

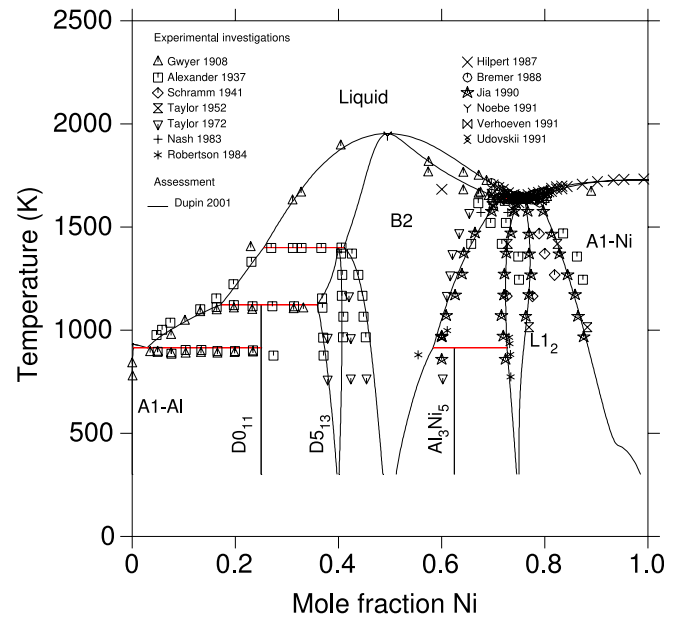


Fig. 1. The CALPHAD phase diagram from Dupin et al. [10], based on experimental and calculated thermodynamic and phase diagram data [11–24].

Goiri and Van der Ven [25] considered the phase stability of various compounds in this system, and van de Walle et al. [26] considered the application of high-throughput calculations to CALPHAD phase diagrams, including some consideration of the short range ordering in the fcc phases of the aluminium-nickel system. Another recent work from Bhattacharyya et al. [27] demonstrates a first-principles phase field method (PFM) for the aluminium-nickel system that can be used to determine the phase boundaries and hence produce the phase diagram. Older first-principles calculations of the phase diagram includes work from Pasturel et al. [28] that uses linear muffin-tin orbitals total energy (LMTO) calculations in combination with cluster variation method (CVM) calculations. Although each of these approaches has drawbacks, be it an inability to fully reproduce the phase diagram, limitations in accuracy, or computational expense, the rich history of investigation in this system provides vast insight that was used to inform the calculations done in this work.

3. Gibbs energy models

Conventional CALPHAD modelling uses the Bragg-Williams [29] point approximation of configurational entropy to describe ideal solution mixing, and any deviations from the ideal solution behaviour are contained within the excess energy terms that are generally parameterised considering experimental data. However, using only first-principles calculations, such excess energy terms are difficult to obtain. The Bragg-Williams configurational entropy approximation is known to be insufficient to describe the real case, for example in over-estimating order-disorder transition temperatures and by excluding any short range ordering [30]. Methods such as the CVM [31] have been used to include higher order cluster contributions to the configurational entropy, which have been shown to improve the theoretical description [28]. However, in real multicomponent systems, the CVM truncation required to provide sufficient accuracy is often computationally infeasible and cannot be easily used directly in computational thermodynamic software. Instead, Kusoffsky et al. [32] demonstrated that using the Bragg-Williams-Gorsky (BWG) pair interaction model [29,33] to obtain reciprocal interaction parameters creates an approximation to the short range ordering behaviour in the fcc system, approximating the Gibbs energy from an equivalent CVM calculation in the tetrahedron approximation.

Table 1

Phases that were considered in this calculation of the Al-Ni phase diagram.

Phase	Stoichiometric composition (at.% Ni)	Strukturbericht	Pearson Symbol	Space Group	Prototype
γ -Al	0	A1	cF4	Fm $\bar{3}$ m	Cu
Al ₃ Ni	25	D0 ₁₁	oP16	Pnma	Fe ₃ C
Al ₃ Ni ₂	40	D5 ₁₃	hP5	P $\bar{3}$ m1	Al ₃ Ni ₂
Al ₄ Ni ₃	42.9			Ia3d	Ni ₄ Ga ₃
β -AlNi	50	B2	cP2	Pm $\bar{3}$ m	CsCl
Al ₃ Ni ₅	62.5		oC16/oS16	Cmmm	Ga ₃ Pt ₅
γ' -AlNi ₃	75	L1 ₂	cP4	Pm $\bar{3}$ m	AuCu ₃
γ -Ni	100	A1	cF4	Fm $\bar{3}$ m	Cu
Liquid					

In this work the stable A1, L1₂, B2, and D5₁₃ phases, and metastable L1₀, D0₃, B32, and A2 phases are considered via the use of the energy of each structure in a pair approximation according to the BWG model to obtain reciprocal interaction parameters within a four substitutional sublattice order-disorder partitioning model framework.

3.1. Four substitutional sublattice order-disorder partitioning model

The order-disorder partitioning model has been widely used to separately describe ordered and corresponding disordered phases that are intrinsically connected by means of an ordering energy. This ensures that the ordered phase is consistent with the disordered (random solution) phase when certain sublattice occupation conditions are met. In the usual application of this model, the parameters of the ordered and disordered phases are simultaneously optimised considering all available thermodynamic and phase diagram data relating to both phases, where there may not be data relating to both phases available at all points in temperature and composition space. However in this work, the energy of the fully ordered end-members and the disordered phase are independently specified at all compositions and temperatures directly from calculated data. The interaction parameters of the disordered phases are obtained directly from calculations, and the interaction parameters of the ordered phases are also obtained directly from the calculated Gibbs energies via the BWG pair models without any conventional optimisation considering experimental thermodynamic or phase boundary data. To implement the order-disorder partitioning model in this way, it is necessary to extract the ordering energy which parameterises the ordered phase relative to the disordered phase. As there is no simultaneous optimisation of different phases in this work, the relations of the model parameters to the calculated Gibbs energy of a specific ordered sublattice configuration and the calculated Gibbs energy of the disordered phase at the same overall composition must be obtained for the specific descriptions used. This means taking into account the number of interaction parameters in the subregular solution model used for the disordered phase and the BWG model used to provide the interaction parameters of the ordered phase as functions of the end-member Gibbs energies. As the authors are not aware of such a derivation in the published literature, a step-by-step description of this process of obtaining these relations to exactly parameterise both the ordered and disordered phase in the four-sublattice order-disorder partitioning model is provided as a supplementary document to enhance the description in this paper.

3.1.1. Face-centred cubic phases

The fcc disordered solid solution phase can be described using a single sublattice model (Al,Ni). The Gibbs energy was described as a function of the molar fraction of species i , x_i , where i may be Al or Ni. As this is a molar quantity, the sum of the molar fraction of each species must sum to unity.

The end-members of this sublattice model are the pure Al and Ni, which have an A1-type structure. The Gibbs energy of the disordered phase may therefore be written as a substitutional solution model in terms of the Gibbs energy of these end-members, $G_i^{\text{fcc-A1}}$,

$$G_m^{\text{fcc:dis}}(x_i) = \sum_i x_i G_i^{\text{fcc:A1}} + RT \sum_i x_i \ln(x_i) + \sum_i \sum_{j>i} x_i x_j L_{ij}^{\text{fcc:dis}} \quad (1)$$

where $L_{ij}^{\text{fcc:dis}}$ are binary interaction parameters which have a temperature and composition dependence described by a Redlich-Kister polynomial as

$$L_{ij}^{\text{fcc:dis}} = \sum_\nu (x_i - x_j)^\nu \cdot {}^\nu L_{ij}^{\text{fcc:dis}} \quad (2)$$

where ν indicates the order of the Redlich-Kister polynomial and ${}^\nu L_{ij}^{\text{fcc:dis}}$ is a polynomial in temperature.

Within the BWG pair approximation model derived by Kusoffsky et al. [32], the energy of each ordered phase is related to the interaction energies via an approximation of the unlike bond energies. The fcc crystal may be split into equivalent four sublattices which may be represented using a four-sublattice model (Al,Ni)_{1/4}(Al,Ni)_{1/4}(Al,Ni)_{1/4}(Al,Ni)_{1/4}. The four-sublattice model has the possible sublattice occupation ordered end-members (where each sublattice is singularly occupied) fcc-Al (A1), Al₃Ni (L1₂), AlNi (L1₀), AlNi₃ (L1₂), and fcc-Ni (A1). The sublattice construction is shown in more detail in Appendix A. The sublattice site occupations defining the A1, L1₂, and L1₀ structures are shown in Table 2, where the white atoms indicate one atomic species in a binary system, and the grey atoms indicate the other. For each case, each species may be either Al or Ni, although in the case of the L1₀ structure, it is equivalent by symmetry regardless of which species occupies the white and grey sites.

In order to describe the phase, two compositional quantities are used. As well as the overall molar fraction of species i , x_i , the site fraction $y_i^{(s)}$ of species i on sublattice s is also required. The site fractions of each species i on each sublattice s must also sum to unity.

These quantities can be related by

$$x_i = \frac{1}{4} \sum_s y_i^{(s)} \quad (3)$$

The disordered case, $y_i^{(1)} = y_i^{(2)} = y_i^{(3)} = y_i^{(4)} = x_i$, is equivalent to the single sublattice case in the disordered phase. Various other ordered structures may exist based on the fcc lattice, but using only the four-sublattice model, they do not appear as end-members. One example of this is the fcc structure often referred to as the F' phase, which has the condition $y_i^{(1)} = y_i^{(2)} \neq y_i^{(3)} \neq y_i^{(4)}$. This phase appears in the fcc phase diagram based on the four-sublattice model ([32,34]), but cannot be represented as an end-member phase with a binary four-sublattice model and so is not considered here. It is worth noting that by using greater numbers of sublattices within the symmetry of the crystal structure, further ordered phases may be considered in the same way.

A model is used where it is assumed that there is some energy difference between ordered and disordered fcc phases, the ordering energy. In the order-disorder partitioning model, the Gibbs energy of the fcc phase in a given sublattice configuration, $G_m^{\text{fcc}}(y_i^{(s)})$, is represented as the energy of the disordered phase at that composition plus the molar ordering energy, $\Delta G_m^{\text{fcc:ord(4SL)}}(y_i^{(s)})$,

$$G_m^{\text{fcc}}(y_i^{(s)}) = G_m^{\text{fcc:dis}}(x_i) + \Delta G_m^{\text{fcc:ord(4SL)}}(y_i^{(s)}) \quad (4)$$

where

$$\Delta G_m^{\text{fcc:ord(4SL)}}(y_i^{(s)}) = G_m^{\text{fcc:ord(4SL)}}(y_i^{(s)}) - G_m^{\text{fcc:ord(4SL)}}(y_i^{(s)} = x_i) \quad (5)$$

Table 2

The ordered end-members that are possible with a four-sublattice description of an fcc phase. The sublattice conditions are defined according to the site occupation probabilities, $y_i^{(n)}$, of a species i on each sublattice n .

Strukturbericht	Formula	Sublattice condition	No. unlike 1nn bonds per tetrahedron
A1	Al/Ni	$y_i^{(1)} = y_i^{(2)} = y_i^{(3)} = y_i^{(4)}$	0
L1 ₂	Al ₃ Ni/ AlNi ₃	$y_i^{(1)} = y_i^{(2)} = y_i^{(3)} \neq y_i^{(4)}$	3
L1 ₀	AlNi	$y_i^{(1)} = y_i^{(2)} \neq y_i^{(3)} = y_i^{(4)}$	4

These are combined to give

$$G_m^{\text{fcc}}(y_i^{(s)}) = G_m^{\text{fcc:dis}}(x_i) + G_m^{\text{fcc:ord(4SL)}}(y_i^{(s)}) - G_m^{\text{fcc:ord(4SL)}}(y_i^{(s)} = x_i) \quad (6)$$

When the phase is disordered, the molar ordering energy $\Delta G_m^{\text{fcc:ord(4SL)}}(y_i^{(s)})$, or the contribution to the Gibbs energy due to ordering, is zero.

The Gibbs ordering energy of a phase with a given sublattice configuration can be written with a four-sublattice regular solution model as

$$\begin{aligned} G_m^{\text{fcc:ord(4SL)}}(y_i^{(s)}) = & \sum_i \sum_j \sum_k \sum_l y_i^{(1)} y_j^{(2)} y_k^{(3)} y_l^{(4)} G_{ijkl}^{\text{fcc:ord(4SL)}} \\ & + \frac{1}{4} RT \sum_s \sum_i y_i^{(s)} \ln y_i^{(s)} \\ & + \sum_i \sum_{j>i} \sum_{k \geq i} \sum_{l>k} \sum_m \sum_n y_i^{(s)} y_j^{(s)} y_k^{(r)} y_l^{(r)} y_m^{(t)} y_n^{(u)} L_{ijkl,mn}^{\text{fcc:ord(4SL)}} \\ & + \sum_i \sum_{j>i} \sum_k \sum_l \sum_m y_i^{(s)} y_j^{(s)} y_k^{(r)} y_l^{(r)} y_m^{(u)} L_{ijk,l:m}^{\text{fcc:ord(4SL)}} \end{aligned} \quad (7)$$

where the first term describes the mechanical mixing of the stoichiometric end-members in the four-sublattice model described above, and is the composition weighted sum of the Gibbs ordering energy $G_{ijkl}^{\text{fcc:ord(4SL)}}$ of the ordered end-members $ijkl$, where the Gibbs energies are given relative to the pure elements in the fcc-A1 state. The $y_i^{(s)} \ln y_i^{(s)}$ term represents the ideal configurational entropy contribution to the Gibbs energy based on the four-sublattice model, and the $L_{ijkl,mn}^{\text{fcc:ord(4SL)}}$ terms represent the interaction parameters that give a contribution to the Gibbs energy depending on the composition. In this notation, species separated by a comma (e.g. i, j) are mixing on a sublattice, and each sublattice is separated by a colon. The energy contribution arising from the reciprocal four-sublattice parameters $L_{ijkl,mn}^{\text{fcc:ord(4SL)}}$ may be considered a first approximation to a contribution to the Gibbs energy due to short range ordering [35].

As all four sublattices are equivalent by crystallographic symmetry, there are various permutations of the Gibbs energy of the end-member occupations.

$$G_{A1-A4}^{\text{fcc:ord(4SL)}} = G_{A:A:A:A}^{\text{fcc:ord(4SL)}} \quad (8)$$

$$G_{L12-A3B}^{\text{fcc:ord(4SL)}} = G_{A:A:A:B}^{\text{fcc:ord(4SL)}} = G_{A:A:B:A}^{\text{fcc:ord(4SL)}} = \dots \quad (9)$$

$$G_{L10-A2B2}^{\text{fcc:ord(4SL)}} = G_{A:A:B:B}^{\text{fcc:ord(4SL)}} = G_{A:B:A:B}^{\text{fcc:ord(4SL)}} = \dots \quad (10)$$

where the same relations may be used for the other $L12$ and $A1$ compounds $G_{L12-AB3}^{\text{fcc:ord(4SL)}}$ and $G_{A1-B4}^{\text{fcc:ord(4SL)}}$.

Following Kusoffsky et al. [32], Abe and Shimono [34], and Lindahl et al. [36], it is further assumed that the ordering energy in a compound is described well when considered as arising from the formation of its unlike nearest-neighbour bonds. This assumption is common in CALPHAD modelling where all energies are given with reference to elemental reference states. Therefore from the tetrahedron construction the fully ordered structures mentioned above are considered in terms of the number of unlike first nearest neighbour (1nn) bonds.

If the energy of the A-B bond is u_{AB}^{fcc} , a general expression for the energy of these intermediate compounds with reference to the A1 states may be written as

$$G_{L12-A3B}^{\text{fcc:ord(4SL)}} = 3u_{AB}^{\text{fcc}} + 3\alpha^{\text{fcc}} \quad (11)$$

$$G_{L10-A2B2}^{\text{fcc:ord(4SL)}} = 4u_{AB}^{\text{fcc}} \quad (12)$$

$$G_{L12-AB3}^{\text{fcc:ord(4SL)}} = 3u_{AB}^{\text{fcc}} + 3\beta^{\text{fcc}} \quad (13)$$

where α^{fcc} and β^{fcc} are parameters representing the asymmetry of the A-B system that may occur due to higher-order interactions not considered in this pair model. If total energies of these three ordered compounds are known relative to the pure elements in their fcc state, all of the parameters in this model may be obtained.

Reciprocal interaction parameters defined by Kusoffsky et al. [32] are used to relate the Gibbs energies for the end-members above to the 1nn interaction energy, $L_{ijk,l:m:n}^{\text{fcc:ord(4SL)}}$, where the subscript denotes the interactions described by that interaction parameter. $L_{ijk,l:m:n}^{\text{fcc:ord(4SL)}}$ therefore describes the simultaneous interaction of i and j on one sublattice and k and l on another, while the third and fourth sublattices are occupied by species m and n respectively. An approximation is made whereby such interaction energy is equivalent to the A-B bond energy u_{AB}^{fcc} as such reciprocal interaction always changes the number of unlike bonds by one. This term represents mixing among first nearest neighbour atoms, and can be obtained from the $G_{ijkl}^{\text{fcc:ord(4SL)}}$. Following Kusoffsky et al. [32], it is also assumed that all interaction parameters with simultaneous interactions on two sites are equivalent and independent of the occupation of the other two sites, e.g.

$$L_{ijk,l:m:n}^{\text{fcc:ord(4SL)}} = L_{A,B:A,B:*}^{\text{fcc:ord(4SL)}} \quad (14)$$

where $*$ represents any possible constituent.

A corresponding approximation may also be made for the 2nn interaction parameters where v_{AB}^{fcc} corresponds to the second nearest neighbour A-B bond energy, equivalent to the switching of atoms between the same sublattice site in neighbouring tetrahedra. The interaction parameter $L_{ijk,l:m}^{\text{fcc:ord(4SL)}}$ (mixing on a single sublattice) is equivalent to this second nearest neighbour interaction. As in the previous case, as Kusoffsky et al. [32], it is assumed that the interaction energy is independent of the species occupying the other sublattices. These terms are not assigned values in this model, as the short range ordering in the ordered phases can be described in a first approximation by the reciprocal interaction parameters only [35], with further interactions accounted for by the interaction parameters for the disordered part, $L_{ij}^{\text{fcc:dis}}$ [32]. Therefore, it is assumed that all interaction parameters with interaction on a single site are equivalent and equal to zero:

$$L_{ij,k:l:m}^{\text{fcc:ord(4SL)}} = 0 \quad (15)$$

In the fcc four substitutional sublattice order-disorder model, a Gibbs energy contribution due to ordering is added to the disordered phase to create the total energy. The $G_{A1-A4}^{\text{fcc:ord(4SL)}}$, $G_{L12-A3B}^{\text{fcc:ord(4SL)}}$, etc, are the parameters of the four-sublattice description, and represent the contribution due to ordering of a fully ordered phase in the particular sublattice configuration, which is distinct from both the energy of the ordered phase $G_m^{\text{fcc:ord(4SL)}}(y_i^{(s)})$ at a particular fractional site occupancy, and the energy of the disordered phase, $G_m^{\text{fcc:dis}}(x_i)$ at a given overall composition. Therefore $G_{A1-A4}^{\text{fcc:ord(4SL)}}$ and $G_{L12-A3B}^{\text{fcc:ord(4SL)}}$ are necessarily 0, as required for the description of the ordering contribution to the Gibbs energy.

Within this formalism it is possible to separately describe the ordered and disordered phases with various end-member energies and interaction parameters. In such cases as this study, where the required Gibbs energy functions are available from first-principles for both the ordered and disordered phases, one must be careful to correctly include such energies in the database.

From equation (6), the total energy of the fully ordered phases $G_m^{\text{fcc}}(y_i^{(s)})$ at the x_A values and sublattice configurations being considered (end members of the four-sublattice model where each sublattice is fully occupied by a single species) is therefore

$$\begin{bmatrix} G_m^{\text{fcc}}(y_A^{(s)} := A1; x_A = 1) \\ G_m^{\text{fcc}}(y_A^{(s)} := L1_2; x_A = \frac{3}{4}) \\ G_m^{\text{fcc}}(y_A^{(s)} := L1_0; x_A = \frac{1}{2}) \\ G_m^{\text{fcc}}(y_A^{(s)} := L1_2; x_A = \frac{1}{4}) \\ G_m^{\text{fcc}}(y_A^{(s)} := A1; x_A = 0) \end{bmatrix} = \begin{bmatrix} G_m^{\text{fcc:dis}}(x_A = 1) \\ G_m^{\text{fcc:dis}}(x_A = \frac{3}{4}) \\ G_m^{\text{fcc:dis}}(x_A = \frac{1}{2}) \\ G_m^{\text{fcc:dis}}(x_A = \frac{1}{4}) \\ G_m^{\text{fcc:dis}}(x_A = 0) \end{bmatrix} + \begin{bmatrix} G_m^{\text{fcc:ord(4SL)}}(y_A^{(s)} := A1; x_A = 1) \\ G_m^{\text{fcc:ord(4SL)}}(y_A^{(s)} := L1_2; x_A = \frac{3}{4}) \\ G_m^{\text{fcc:ord(4SL)}}(y_A^{(s)} := L1_0; x_A = \frac{1}{2}) \\ G_m^{\text{fcc:ord(4SL)}}(y_A^{(s)} := L1_2; x_A = \frac{1}{4}) \\ G_m^{\text{fcc:ord(4SL)}}(y_A^{(s)} := A1; x_A = 0) \end{bmatrix} - \begin{bmatrix} G_m^{\text{fcc:ord(4SL)}}(y_A^{(s)} = x_A = 1) \\ G_m^{\text{fcc:ord(4SL)}}(y_A^{(s)} = x_A = \frac{3}{4}) \\ G_m^{\text{fcc:ord(4SL)}}(y_A^{(s)} = x_A = \frac{1}{2}) \\ G_m^{\text{fcc:ord(4SL)}}(y_A^{(s)} = x_A = \frac{1}{4}) \\ G_m^{\text{fcc:ord(4SL)}}(y_A^{(s)} = x_A = 0) \end{bmatrix} \quad (16)$$

where the notation $(y_A^{(s)} := L1_2; x_A = \frac{3}{4})$ indicates that the sublattice population fulfils the condition of the $L1_2$ phase as given in Table 2, while the overall composition is $x_A = \frac{3}{4}$. The ordering contribution under these conditions when fully ordered are the parameters included in the model e.g. $G_m^{\text{fcc:ord(4SL)}}(y_A^{(s)} := L1_2; x_A = \frac{3}{4}) = G_{L1_2-A_3B}^{\text{fcc:ord(4SL)}}$. This may be rearranged to express the parameters of the four sublattice order-disorder partitioning model as a function of the ordering energy of the fully ordered phases as

where $\underline{\mathbf{M}}^{\text{fcc}}$ represents the matrix connecting the total energies of the ordered end-member phases and the total energies of the disordered phase at various compositions (which may both be calculated from first-principles) to the parameters in the four-sublattice order-disorder model. $\underline{\mathbf{M}}^{\text{fcc}}$ is dependent on the choice of models used, e.g. the number of interaction parameters in the disordered phase, and the relation between the end-member energies and the four sublattice interaction parameters.

Therefore, if the total energies of the ordered and disordered phase are known from first-principles or assessment, the parameters for the model may be obtained by inverting matrix $\underline{\mathbf{M}}^{\text{fcc}}$.

In the case derived from the Bragg-Williams-Gorsky model where

$$L_{A,B:A,B,*}^{\text{fcc:ord(4SL)}} = \frac{1}{4} G_{L1_0-A_2B_2}^{\text{fcc:ord(4SL)}} \quad (18)$$

and

$$L_{A,B:*,*}^{\text{fcc:ord(4SL)}} = 0 \quad (19)$$

$$\begin{bmatrix} G_m^{\text{fcc}}(y_A^{(s)} := A1; x_A = 1) \\ G_m^{\text{fcc}}(y_A^{(s)} := L1_2; x_A = \frac{3}{4}) \\ G_m^{\text{fcc}}(y_A^{(s)} := L1_0; x_A = \frac{1}{2}) \\ G_m^{\text{fcc}}(y_A^{(s)} := L1_2; x_A = \frac{1}{4}) \\ G_m^{\text{fcc}}(y_A^{(s)} := A1; x_A = 0) \end{bmatrix} - \begin{bmatrix} G_m^{\text{fcc:dis}}(x_A = 1) \\ G_m^{\text{fcc:dis}}(x_A = \frac{3}{4}) \\ G_m^{\text{fcc:dis}}(x_A = \frac{1}{2}) \\ G_m^{\text{fcc:dis}}(x_A = \frac{1}{4}) \\ G_m^{\text{fcc:dis}}(x_A = 0) \end{bmatrix} = \underline{\mathbf{M}}^{\text{fcc}} \begin{bmatrix} G_{A1-A_4}^{\text{fcc:ord(4SL)}} \\ G_{L1_2-A_3B}^{\text{fcc:ord(4SL)}} \\ G_{L1_0-A_2B_2}^{\text{fcc:ord(4SL)}} \\ G_{L1_2-AB_3}^{\text{fcc:ord(4SL)}} \\ G_{A1-B_4}^{\text{fcc:ord(4SL)}} \end{bmatrix} \quad (17)$$

the matrix $\underline{\underline{\mathbf{M}}}^{\text{fcc}}$ is

where, $u_{\text{AB}}^{\text{bcc}}$ and $v_{\text{AB}}^{\text{bcc}}$ are the 1nn and 2nn bond energy respectively, and as for the fcc case, parameters ω_1^{bcc} and ω_2^{bcc} are introduced to account for the asymmetry that may occur due to higher order interactions.

$$\underline{\underline{\mathbf{M}}}^{\text{fcc}} = \begin{bmatrix} 0 & 0 & 0 & 0 & 0 \\ -\left(\frac{3}{4}\right)^4 & 1 - 4\left(\frac{3}{4}\right)^3\left(\frac{1}{4}\right) & -6\left(\frac{3}{4}\right)^2\left(\frac{1}{4}\right)^2 - \frac{1}{4}\left[6\left(\frac{3}{4}\right)^4\left(\frac{1}{4}\right)^2 + 12\left(\frac{3}{4}\right)^3\left(\frac{1}{4}\right)^3 + 6\left(\frac{3}{4}\right)^2\left(\frac{1}{4}\right)^4\right] & -4\left(\frac{3}{4}\right)\left(\frac{1}{4}\right)^3 & -\left(\frac{1}{4}\right)^4 \\ -\left(\frac{1}{2}\right)^4 & -4\left(\frac{1}{2}\right)^4 & 1 - 6\left(\frac{1}{2}\right)^4 - 24\left(\frac{1}{4}\right)\left(\frac{1}{2}\right)^6 & -4\left(\frac{1}{2}\right)^4 & -\left(\frac{1}{2}\right)^4 \\ -\left(\frac{1}{4}\right)^4 & -4\left(\frac{1}{4}\right)^3\left(\frac{3}{4}\right) & -6\left(\frac{1}{4}\right)^2\left(\frac{3}{4}\right)^2 - \frac{1}{4}\left[6\left(\frac{1}{4}\right)^4\left(\frac{3}{4}\right)^2 + 12\left(\frac{1}{4}\right)^3\left(\frac{3}{4}\right)^3 + 6\left(\frac{1}{4}\right)^2\left(\frac{3}{4}\right)^4\right] & 1 - 4\left(\frac{1}{4}\right)\left(\frac{3}{4}\right)^3 & -\left(\frac{3}{4}\right)^4 \\ 0 & 0 & 0 & 0 & 0 \end{bmatrix} \quad (20)$$

3.1.2. Body-centred cubic phases

The above inverted matrix method of assigning parameters describing both the ordered and disordered phases directly from first-principles calculations is applied to the bcc four sublattice order-disorder model as derived by Abe and Shimono [34] in a similar way to the fcc phase described in Section 3.1.1.

A similar pair approximation is applied to tetrahedron structures representing bcc phases, but while fcc phases have a single lattice parameter defining the volume, the asymmetry of the a and c lattice parameter in the conventional bcc unit cell means that the six bonds within the tetrahedron are of either 1nn and 2nn type, and the bonds between equivalent sites on neighbouring tetrahedra are of third nearest neighbour (3nn) type. The sublattice construction is described in more detail in Appendix A. The end-member ordered phases for the bcc four-sublattice model are Al (A2), Al₃Ni (D0₃), AlNi (B2), AlNi (B32), AlNi₃ (D0₃), and Ni (A2). The sublattice site occupation conditions defining each phase are given in Table 3, where as before, one species is represented by white atoms, and another by grey.

The end-member energies relative to the pure elements in the A2 structure can be written:

$$G_{\text{D0}_3-\text{A}_3\text{B}}^{\text{bcc:ord(4SL)}} = 2u_{\text{AB}}^{\text{bcc}} + 1.5v_{\text{AB}}^{\text{bcc}} + \omega_1^{\text{bcc}} \quad (21)$$

$$G_{\text{B2}-\text{A}_2\text{B}_2}^{\text{bcc:ord(4SL)}} = 4u_{\text{AB}}^{\text{bcc}} \quad (22)$$

$$G_{\text{B32}-\text{A}_2\text{B}_2}^{\text{bcc:ord(4SL)}} = 2u_{\text{AB}}^{\text{bcc}} + 3v_{\text{AB}}^{\text{bcc}} \quad (23)$$

$$G_{\text{D0}_3-\text{AB}_3}^{\text{bcc:ord(4SL)}} = 2u_{\text{AB}}^{\text{bcc}} + 1.5v_{\text{AB}}^{\text{bcc}} + \omega_2^{\text{bcc}} \quad (24)$$

Reciprocal interaction parameters for the four-sublattice order-disorder partitioning model may be defined using these 1nn and 2nn bond energies such as in the fcc case, although not via a simple linear relation [34]. To consider the permutations of the interaction parameters, it is important to remember that not all sites are equivalent, and therefore for the case of simultaneous interaction on two sublattices, it is significant which two sublattices are involved in the exchange. The sublattices may be separated into two pairs of equivalent sublattices: the first two sublattices and the second two sublattices. If there is simultaneous interaction on two sublattices in the same pair, it is related to the second nearest neighbour interaction parameter $L_{\text{A,B:A,B};ij}^{\text{bcc:ord(4SL)}}$ (where the other sites are occupied by species i and j). If there is simultaneous interaction on two sublattices that are not in the same set, it is related to the first nearest neighbour interaction parameter $L_{\text{A,B:A,B};jk}^{\text{bcc:ord(4SL)}}$. The 3nn interaction parameter $L_{\text{A,B:A,B};jk}^{\text{bcc:ord(4SL)}}$ (interaction on a single sublattice site) may additionally related to the 3nn A-B bond energy but was not assigned a value in this model.

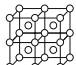



Abe and Shimono [34] consider the effect of short range ordering in the 1nn and 2nn shell and obtain approximate expressions for the 1nn and 2nn reciprocal interaction parameters as a function of the 1nn and 2nn bond energy,

$$L_{\text{A,B:A,B};*}^{\text{bcc:ord(4SL)}} = \frac{1}{2}u_{\text{AB}}^{\text{bcc}} \leq 0 \quad (25)$$

$$L_{\text{A,B:A,B};*}^{\text{bcc:ord(4SL)}} = \frac{3(v_{\text{AB}}^{\text{bcc}})^2}{4u_{\text{AB}}^{\text{bcc}}} \leq 0 \quad (26)$$

Table 3

The ordered end-members that are possible with a four-sublattice description of a bcc phase.

Strukturbericht	Formula	Sublattice condition		No. unlike 1nn bonds per tetrahedron	No. unlike 2nn bonds per tetrahedron
A2	Al/Ni	$y_i^{(1)} = y_i^{(2)} = y_i^{(3)} = y_i^{(4)}$		0	0
B2	AlNi	$y_i^{(1)} = y_i^{(2)} \neq y_i^{(3)} = y_i^{(4)}$		4	0
B32	AlNi	$y_i^{(1)} = y_i^{(3)} \neq y_i^{(2)} = y_i^{(4)}$		2	2
D0 ₃	Al ₃ Ni/AlNi ₃	$y_i^{(1)} \neq y_i^{(2)} = y_i^{(3)} = y_i^{(4)}$		2	1

that may be used.

As the procedure is very similar to the fcc case, the definition of the four sublattice order-disorder model is not repeated here. In the bcc case, as all four sublattices are not equivalent, there are two ordered phases with 50% composition, B2 and B32. Both of these phases are represented within the model. If the total energy of the ordered and disordered phase are known from first-principles or assessment, the parameters for the model may be obtained by inverting matrix $\underline{\mathbf{M}}^{\text{bcc}}$ which relates the four-sublattice model parameters to the ordering energy of each fully ordered phase represented by the sublattice model as

$$\begin{bmatrix} G_{\text{A2-A}_4}^{\text{bcc:ord(4SL)}} \\ G_{\text{D0}_3\text{-A}_3\text{B}}^{\text{bcc:ord(4SL)}} \\ G_{\text{B2-A}_2\text{B}_2}^{\text{bcc:ord(4SL)}} \\ G_{\text{B32-A}_2\text{B}_2}^{\text{bcc:ord(4SL)}} \\ G_{\text{D0}_3\text{-AB}_3}^{\text{bcc:ord(4SL)}} \\ G_{\text{A2-B}_4}^{\text{bcc:ord(4SL)}} \end{bmatrix} = \left(\underline{\mathbf{M}}^{\text{bcc}} \right)^{-1} \begin{bmatrix} G_m^{\text{bcc}} \left(y_A^{(s)} := \text{A2}; x_A = 1 \right) \\ G_m^{\text{bcc}} \left(y_A^{(s)} := \text{D0}_3; x_A = \frac{3}{4} \right) \\ G_m^{\text{bcc}} \left(y_A^{(s)} := \text{B2}; x_A = \frac{1}{2} \right) \\ G_m^{\text{bcc}} \left(y_A^{(s)} := \text{B32}; x_A = \frac{1}{2} \right) \\ G_m^{\text{bcc}} \left(y_A^{(s)} := \text{D0}_3; x_A = \frac{1}{4} \right) \\ G_m^{\text{bcc}} \left(y_A^{(s)} := \text{A2}; x_A = 0 \right) \end{bmatrix} - \begin{bmatrix} G_m^{\text{bcc:dis}}(x_A = 1) \\ G_m^{\text{bcc:dis}}\left(x_A = \frac{3}{4}\right) \\ G_m^{\text{bcc:dis}}\left(x_A = \frac{1}{2}\right) \\ G_m^{\text{bcc:dis}}\left(x_A = \frac{1}{2}\right) \\ G_m^{\text{bcc:dis}}\left(x_A = \frac{1}{4}\right) \\ G_m^{\text{bcc:dis}}(x_A = 0) \end{bmatrix} \quad (27)$$

where the G_m^{bcc} represent the calculable molar Gibbs energy of the end-member ordered phases with particular composition and sublattice configuration, $G_m^{\text{bcc:dis}}$ represent the molar energy of the disordered phase at a particular composition, and $\underline{\mathbf{M}}^{\text{bcc}}$ depends on the four-sublattice 1nn and 2nn interaction parameters of the ordering energies.

However, in separating the known ordering and disordered contributions to the Gibbs energy within the four substitutional sublattice order-disorder model, with the approximations for the first and second nearest neighbour interaction energies provided by Abe and Shimono [34] (equations (25) and (26)), it is not possible to exactly specify both the energy of the ordered phases and disordered phase because the four-sublattice interaction parameters cannot be expressed as linear combinations of the Gibbs energies. The approximation from Abe and Shimono is intended to describe the interaction parameters of the ordered phase when a symmetrical approximation for the disordered phase is used. However, Lindahl et al. [36] found that it was effective to introduce interaction energies in the ordered phases implicitly by use of an asymmetric disordered phase description, where the interaction

parameters of the ordering energy that are added to the contributions from the disordered phase assume ideality. In the order-disorder partitioning model, the interactions of the phases described by four sublattices have energy and interaction energy contributions from both the disordered part and the ordering energy part. Therefore the total reciprocal interaction energy (which may be considered an approximation to the energy contribution due to short range ordering [35]) has a finite value if the disordered phase is non-ideal, even if the ordering energy contribution to the reciprocal interaction parameters is zero. As the disordered phase is described from first-principles calculations in this work, the non-ideal interactions may be described by the contri-

butions from the disordered phase at all temperatures. The exact knowledge of this energy, which may not be typically experimentally known, allows use of the inverted matrix approach which approximates the reciprocal interaction parameter contribution from the ordering energy as zero.

The composition dependence of the Gibbs energy of the B2 phase was found to be very similar when described only from the disordered interaction parameters compared to when described using the reciprocal interaction parameters derived by Abe and Shimono [34] without the exact description of the disordered phase. Both models found that the contribution to the Gibbs energy of the B2 phase from the reciprocal interactions was very small and did not significantly affect the phase diagram topology. The agreement between these two models allows the conclusion that, at least in this case, an approximation of the effects of short range ordering in the ordered phases may be described with the order-disorder partitioning model via the interactions in the disordered phase.

With this assumption that all four-sublattice interaction parameters for the order-disorder partitioning model can be set as zero, the matrix $\underline{\mathbf{M}}^{\text{bcc}}$ is given by

$$\underline{\mathbf{M}}^{\text{bcc}} = \begin{bmatrix} 0 & 0 & 0 & 0 & 0 & 0 \\ -\left(\frac{3}{4}\right)^4 & 1 - 4\left(\frac{3}{4}\right)^3\left(\frac{1}{4}\right) & -2\left(\frac{3}{4}\right)^2\left(\frac{1}{4}\right)^2 & -4\left(\frac{3}{4}\right)^2\left(\frac{1}{4}\right)^2 & -4\left(\frac{3}{4}\right)\left(\frac{1}{4}\right)^3 & -\left(\frac{1}{4}\right)^4 \\ -\left(\frac{1}{2}\right)^4 & -4\left(\frac{1}{2}\right)^4 & 1 - 2\left(\frac{1}{2}\right)^4 & -4\left(\frac{1}{2}\right)^4 & -4\left(\frac{1}{2}\right)^4 & -\left(\frac{1}{2}\right)^4 \\ -\left(\frac{1}{2}\right)^4 & -4\left(\frac{1}{2}\right)^4 & -2\left(\frac{1}{2}\right)^4 & 1 - 4\left(\frac{1}{2}\right)^4 & -4\left(\frac{1}{2}\right)^4 & -\left(\frac{1}{2}\right)^4 \\ -\left(\frac{1}{4}\right)^4 & -4\left(\frac{1}{4}\right)^3\left(\frac{3}{4}\right) & -2\left(\frac{1}{4}\right)^2\left(\frac{3}{4}\right)^2 & -4\left(\frac{1}{4}\right)^2\left(\frac{3}{4}\right)^2 & 1 - 4\left(\frac{1}{4}\right)\left(\frac{3}{4}\right)^3 & -\left(\frac{3}{4}\right)^4 \\ 0 & 0 & 0 & 0 & 0 & 0 \end{bmatrix} \quad (28)$$

3.2. Hexagonal (D5₁₃) phase

The hexagonal D5₁₃ phase was modelled with two substitutional sublattices (Al,Ni)₃(Al,Ni)₂ based on the Wagner-Schottky defect model [37], where the Gibbs energy may be expressed as a function of the fractional site occupancy of species *i* on sublattice *s*,

$$G_m^{D5_{13}}(y_i^{(s)}) = \sum_i \sum_j y_i^{(1)} y_j^{(2)} \cdot G_{ij}^{D5_{13}} + \frac{1}{2} RT \sum_s \sum_i y_i^{(s)} \ln(y_i^{(s)}) + \sum_i \sum_{j>i} \sum_k y_i^{(s)} y_j^{(s)} y_k^{(t)} L_{ijk}^{D5_{13}} + \sum_i \sum_{j>i} \sum_{k \geq i} \sum_{l>k} y_i^{(s)} y_j^{(s)} y_k^{(t)} y_l^{(t)} L_{ijkl}^{D5_{13}} \quad (29)$$

where the sum of the site fractions of each sublattice sum to unity and the site fraction on each sublattice is related to the overall composition x_i by

$$x_i = \frac{1}{2} \sum_s y_i^{(s)} \quad (30)$$

In the model used in this work, the reciprocal interaction parameter, $L_{ijkl}^{D5_{13}}$ is neglected, and the interaction parameters $L_{ijk}^{D5_{13}}$ are expanded with a Redlich-Kister polynomial

$$L_{ijk}^{D5_{13}} = \sum_\nu (y_i - y_j)^\nu \cdot {}^\nu L_{ijk}^{D5_{13}} \quad (31)$$

where ν indicates the order of the Redlich-Kister polynomial and ${}^\nu L_{ijk}^{D5_{13}}$ is a polynomial in temperature.

The D5₁₃ structure was considered within a BWG framework to introduce a 1nn interaction parameter obtained from the 1nn bond energy. The end-members of this sublattice model are Al, Al₃Ni₂, Al₂Ni₃, and Ni, all in the D5₁₃ structure. The A₃B₂ and A₂B₃ compounds have five unlike 1nn A-B bonds per five atom unit cell.

The calculated energy of the A₃B₂ compound was used to determine the energy of each A-B bond $u_{AB}^{D5_{13}}$ in the Al-rich case, and the energy of the A₂B₃ compound was used to determine the energy of the A-B bond $v_{AB}^{D5_{13}}$ in the Ni-rich case.

$${}^*G_{A_3B_2}^{D5_{13}} - \frac{3}{5} {}^*G_{A_3A_2}^{D5_{13}} - \frac{2}{5} {}^*G_{B_3B_2}^{D5_{13}} = 5u_{AB}^{D5_{13}} \quad (32)$$

$${}^*G_{A_2B_3}^{D5_{13}} - \frac{2}{5} {}^*G_{A_3A_2}^{D5_{13}} - \frac{3}{5} {}^*G_{B_3B_2}^{D5_{13}} = 5v_{AB}^{D5_{13}} \quad (33)$$

The 1nn interaction energies affecting each compound were therefore introduced for the Al-rich and Ni-rich cases as being directly equivalent to the 1nn bond energies as

$$L_{A:A,B}^{D5_{13}} = L_{A,B:B}^{D5_{13}} = u_{AB}^{D5_{13}} \quad (34)$$

$$L_{B:A,B}^{D5_{13}} = L_{A,B:A}^{D5_{13}} = v_{AB}^{D5_{13}} \quad (35)$$

3.3. Line compounds

The D0₁₁, Al₃Ni₅, and Al₄Ni₃ phases were modelled as stoichiometric line compounds. For these Al_xNi_y compounds, the sublattice model (Al)_x(Ni)_y was employed. The single end-member of the sublattice model, ${}^*G_m^{Al_xNi_y}(T)$, was calculated for each of the three stoichiometric compounds and used directly in the thermodynamic database.

3.4. Liquid

The liquid description was taken from Ansara et al. [9] and Dupin et al. [10], where a single sublattice substitutional solution model, such as was used for the fcc and bcc disordered solid solution phases, was employed.

$$G_m^{\text{liquid}}(x_i) = \sum_i x_i \cdot G_i^{\text{liquid}} + RT \sum_i x_i \ln(x_i) + \sum_i \sum_{j>i} x_i x_j L_{ij}^{\text{liquid}} \quad (36)$$

where the excess energy is expanded with a fourth order Redlich-Kister polynomial

$$L_{ij}^{\text{liquid}} = \sum_{\nu=0}^4 (x_i - x_j)^\nu \cdot {}^\nu L_{ij}^{\text{liquid}} \quad (37)$$

with

$${}^\nu L_{ij}^{\text{liquid}} = {}^\nu A + {}^\nu B T \quad (38)$$

where ${}^\nu A$ and ${}^\nu B$ are constant coefficients.

4. First-principles calculations

4.1. Computational details

First-principles calculations were performed for solid ordered end-member phases and disordered fcc and bcc solid solution phases. Calculations considering the liquid phase directly were not performed and in the results shown the liquid description from Dupin et al. [10] is used to provide a point of comparison with the experiment-based phase diagram. The solid-only phase diagram, using only calculated data, is also shown in Section 5. The crystal structures for the ordered phases were produced from the known prototypes. Special Quasirandom Structures (SQS) [38] provide a structure that may be considered as an approximation of the disordered state. The disordered fcc and bcc phases were modelled using SQS which can be generated at various compositions by the mcsqs code in the ATAT package [39]. In this work, SQS for fcc and bcc were considered at intermediate composition intervals of 12.5% across the composition range of 0–100 at.%Ni (12.5, 25, 37.5, 50, 62.5, 75, 87.5 at.% Ni). The SQS at 25, 50, and 75 at.% Ni were adopted from Wolverton [40] and Jiang et al. [41] in which their supercells contain 16 atoms. The remaining SQS supercells were generated as part of this work, consisting of 64 atoms.

The total Gibbs energy, $G^{\text{total}}(T)$, can be expressed as the summation of the energy of electrons at 0 K and the contributions of the various finite temperature effects,

$$G^{\text{total}}(T) = G^{\text{GS}}(0 \text{ K}) + G^{\text{vib}}(T) + G^{\text{el}}(T) \quad (39)$$

where $G^{\text{GS}}(0 \text{ K})$ is the ground state (GS) energy at 0 K, $G^{\text{vib}}(T)$ is the thermal vibrational contribution, and $G^{\text{el}}(T)$ is the thermal electronic contribution.

To obtain the GS energy of each ordered phase, $G^{\text{GS}}(0 \text{ K})$, spin-polarised DFT calculations were performed using the Projector Augmented Wave (PAW) method [42] as implemented in the Vienna Ab initio Software Package (VASP) [43–45]. The Generalized Gradient Approximation and the Perdew-Burke-Ernzerhof pseudopotential (GGA-PBE) [46,47] were used in treating the exchange and correlation energy. An energy cutoff wavefunction was set up at 560 eV and a Monkhorst-Pack mesh [48] of more than 5000 *k*-points per unit cell was used. All ordered structures were fully relaxed until all force components were smaller than 0.002 eV/Å.

Both the vibrational free energy and thermal electronic energy were calculated using the same procedure as Wang et al. [49] and Arroyave et al. [50] for compounds in the Al-Ni system, with the Alloy Theoretic Automated Toolkit (ATAT) package [51].

To obtain the temperature dependent thermal vibrational Gibbs energy, $G^{\text{vib}}(T)$, phonon calculations up to 2000 K were performed within the quasiharmonic approximation using the supercell approximation method. The phonon density of states (DOS) was used to fit the Birch-Murnaghan equation of state (EOS). A minimum of four volumes were generated for each structure, and at each volume, different supercells

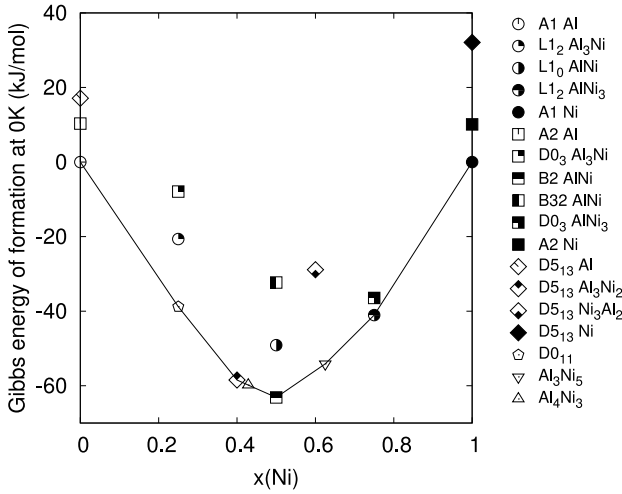


Fig. 2. Calculated Gibbs energies of formation at 0 K, of all ordered phases considered in this work, relative to fcc Al and Ni.

with their corresponding atomic position perturbations were constructed for interatomic force constant calculations. Afterwards, dynamical matrices were built and phonon frequencies and density were obtained by diagonalising the dynamical matrices. The vibrational free energy contributions at each volume, $F^{\text{vib}}(T)$, were then calculated directly from the phonon frequencies and density of states with

$$F^{\text{vib}}(T) = k_B T \int_0^\infty \ln \left[2 \sinh \left(\frac{h\nu}{2k_B T} \right) \right] g(\nu) d\nu \quad (40)$$

where ν are the frequencies of the allowed modes of oscillations, $g(\nu)$ is the phonon DOS, h is the Planck constant and k_B is the Boltzmann constant [50].

The thermal electronic free energy, F^{el} , is calculated from the configurational entropy between the electrons excited to the states above the Fermi energy, ε_F , and the electrons that remain below the Fermi energy. This thermal electronic entropy is calculated from the electronic DOS, $n(\varepsilon, V)$, which is a function of energy ε and volume V , and the Fermi distribution function, f , with

$$S^{\text{el}}(V, T) = -k_B N \int n(\varepsilon, V) [f \ln f + (1-f) \ln (1-f)] d\varepsilon \quad (41)$$

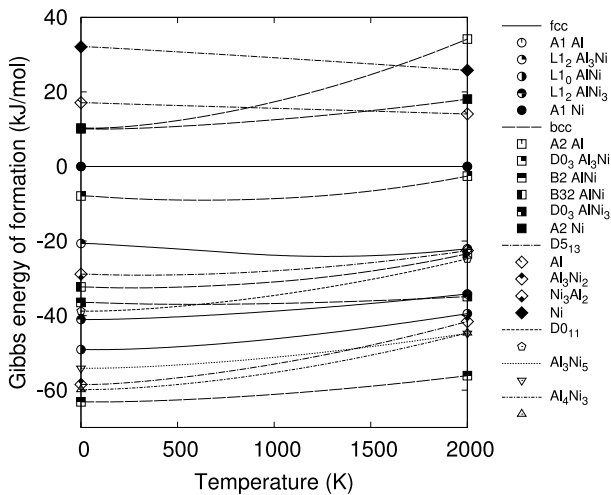


Fig. 3. Calculated Gibbs energies of formation of all ordered phases considered in this work, between 0 K and 2000 K, relative to fcc Al and Ni at each temperature.

Since

$$E^{\text{el}}(V, T) = \int n(\varepsilon, V) f \varepsilon d\varepsilon - \int n(\varepsilon, V) \varepsilon d\varepsilon \quad (42)$$

the thermal electronic free energy can be obtained using

$$F^{\text{el}} = E^{\text{el}} - TS^{\text{el}} \quad (43)$$

The Helmholtz free energy $F(V, T)$ is obtained by combining each of the above contributions with

$$F(V, T) = E^0(V) + F^{\text{vib}}(V, T) + F^{\text{el}}(V, T) \quad (44)$$

The energies are considered at various volumes, and the total free energy can therefore be minimised with respect to volume at each temperature to obtain the equilibrium volume at each temperature, $V^*(T)$. Therefore the temperature dependent Helmholtz free energy becomes

$$F(T) = E(V^*(T)) + F^{\text{vib}}(V^*(T), T) + F^{\text{el}}(V^*(T), T) \quad (45)$$

At atmospheric pressure, the PV term in the Gibbs energy can be neglected, and the Helmholtz free energy is used as $G^{\text{total}}(T)$ in the phase diagram calculations.

For the disordered phases, the Debye-Grüneisen model was used to obtain the temperature dependence of the thermal vibrational Gibbs energy contribution due to the prohibitive computational cost of performing phonon calculations for such low symmetry structures. The Debye-Grüneisen model has been widely used to obtain the finite temperature contribution to the Gibbs energy for SQS compounds such as by Lieser et al. [52] and Liu et al. [53], and has been shown to reproduce the experimental data well for the Al-Ni system [54]. According to Moruzzi et al. [55], the conventional Debye-Grüneisen model contains a system-specific scaling parameter (with the value of 0.617 obtained for several non-magnetic metals) based on an assumption of the relationship between the sound velocity and the bulk modulus. Nowadays, it is possible to determine the value of this parameter for specific system using the Debye temperature calculated from the 0 K phonon spectrum, as in the work of Shang et al. [54]. In this work, a value of 0.67 was calculated for this parameter for the Al-Ni system.

4.2. Ordered phases

The ground state Gibbs energies of formation of all ordered phases with reference to fcc Al and fcc Ni are shown in Fig. 2.

A consequence of using the Compound Energy Formalism (CEF) sublattice description is that all end-members must be carefully assigned temperature dependent polynomial Gibbs energies, even if they are metastable. In conventional CALPHAD descriptions, such metastable compound energies are designated approximate values by extrapolation or estimation [56], and any deviation of the real case from the resulting ideal solution of phases is swept into the excess energy term, where parameters (that do not directly correspond to any physical properties) are optimised considering the experimental information to give a adequate description. First-principles calculations of metastable end-members often contradict the widely used estimates for elemental stabilities [57,58], and there are significant challenges faced in calculating the temperature dependence of such energies in the case of a phase being dynamically unstable [59].

Most of the required end-members for this system were both dynamically and thermodynamically stable, but some lacked either dynamic and/or thermodynamic stability. Thermodynamic instability is not a problem when performing first-principles calculations, as it only indicates stability relative to a chosen stable elemental state. However, phonon calculations for dynamically unstable phases result in imaginary phonon frequencies that prevent the calculation of any temperature-dependent properties. For some of the metastable end-member compounds required for this system, there was a temperature range where

they were unstable.

The dynamically unstable end-members $\text{D0}_3\text{-Al}_3\text{Ni}$ and B32-AlNi (bcc phases), and pure Al and Ni in the D5_{13} structure had a very small DOS contribution from imaginary phonon frequencies. There are techniques that can sometimes be used to eliminate imaginary phonon frequencies [59], but they were not applied in this case. Since the contribution to the DOS from the imaginary frequencies was small, the imaginary modes in the phonon DOS were ignored for the dynamically unstable phases mentioned above as has been done by Mantina et al. [60,61].

The Gibbs energies for all the ordered phases, obtained by phonon calculations, are shown in Fig. 3.

To be used in a thermodynamic database, the calculated data for each end-member must usually be fit to a function of temperature. The polynomial form of the temperature dependence of the Gibbs energy has long been a topic of heated discussion in the CALPHAD community, particularly with regards to fitting from 0 K to high temperature [62]. Direct least-squares fitting of conventional $G(T)$ functions (such as the kind recommended by Dinsdale [63]) cannot well reproduce calculated Gibbs energy data without manual optimisation and compromise even in a limited temperature range (such as 298 K to the melting point of the pure elements). Other Gibbs energy models exist that allow modelling of the whole temperature range (such as Chen and Sundman [64], and Roslyakova et al. [65]), but as segmented models, they have the disadvantage that it is challenging to avoid discontinuities, as well as requiring some degree of manual optimisation rather than direct fitting.

This work is a theoretical exploration of the ability to calculate a phase diagram from first-principles Gibbs energy data. With this in mind, a very simple quadratic $G(T)$ model (constant C_p) was chosen in this work as it can reproduce the calculated data well across the full temperature range (0–2000 K). While such a database will not correctly reproduce thermodynamic functions dependent on the derivatives of the Gibbs energy (such as entropy and heat capacity), the phase boundaries are appropriately determined. A high quality fit of the calculated Gibbs energy data to a recommended model (such as Chen and Sundman [64]) could theoretically reproduce both the calculated phase diagram obtained in this work, as well as the thermodynamic functions that may be obtained by taking careful numerical derivatives of the calculated data. However, as this work aims only to reproduce the phase diagram with

the minimum manual optimisation of parameters, the simplified Gibbs energy model applied here was deemed sufficient.

All of the end-member Gibbs energies were fitted directly to a second order polynomial function between 0 K and 2000 K using a least-squares method and directly imported into the thermodynamic database (tdb) file used to perform the phase diagram calculation. The calculated pure element energies were used in the database in place of the SGTE pure element energies [63] for consistency and to allow calculation of the phase diagram down to 0 K. However, the SGTE descriptions for Al and Ni were reproduced well by the first-principles calculations, and there are no visible changes to the calculated phase diagram above 298 K when SGTE end member energies are used in place of the calculated pure element energies. Recent development of third generation CALPHAD databases, such as used in assessments such as by Dinsdale et al. [66], may allow future use of SGTE pure element descriptions at low temperature. The interaction parameters describing the excess energy of the ordered phases were all obtained directly from the end-member parameters according to the BWG model described above. All parameters for each phase were fitted directly to the calculated first-principles thermodynamic data for that phase without any optimisation considering the phase boundaries or data relating to other phases.

4.3. Disordered phases

The disordered solid solution phases were considered via SQS calculations at several compositions. As SQS naturally have very low symmetry, it becomes highly computationally expensive to perform phonon calculations to determine the vibrational contribution to the Gibbs energy [67] and therefore calculations of the vibrational contribution to the Gibbs energy for the fcc and bcc SQS were performed using the Debye-Grüneisen model. However, the Debye-Grüneisen model is known to have a lower accuracy than phonon calculations [54], and cannot be used with full confidence at very high temperatures in some systems. Referring to the comparison of Debye-Grüneisen model calculations and phonon calculations for the stable ordered phases, Al-Ni and $\text{L1}_2\text{-AlNi}_3$ from Shang et al. [54], phonon calculations in the quasi-harmonic approximation were performed for fcc SQS at 25%, 50%, and 75% Ni for comparison and validation, and based on these calculations data below 1500 K were used in fitting the Gibbs energies used in the database.

It is not desirable to use data obtained partially from phonon calculations and partly from the Debye-Grüneisen model as data calculated

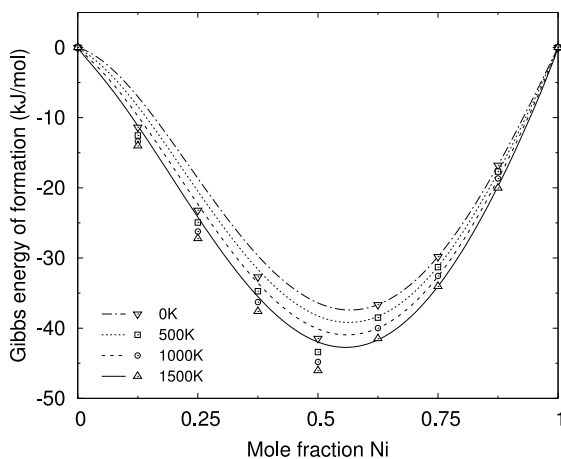


Fig. 4. Gibbs energy of the disordered fcc phase as a function of composition, shown at 500 K temperature intervals between 0 K and 1500 K. The Gibbs energy is given with reference to the fcc (A1) end-members at that temperature. The points show the data calculated from first-principles and the lines show the fitted Gibbs energy. The interaction parameters were determined directly from the excess energy at $x_{\text{Ni}} = 0.625, 0.75$, and 0.875 with no further optimisation. During the fitting procedure, priority was given to reproducing the calculated data on the Ni-rich side as that is the range of stability of the disordered fcc phase.

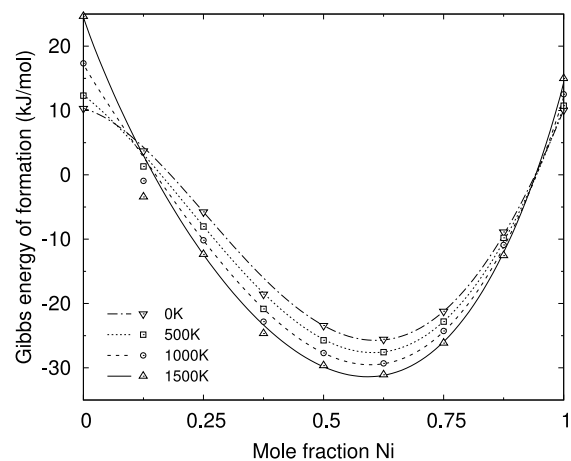


Fig. 5. Gibbs energy of the disordered bcc phase as a function of composition with reference to fcc Al and Ni, shown at 500 K temperature intervals between 0 K and 1500 K. The points show the data calculated from first-principles and the lines show the fitted Gibbs energy. The interaction parameters were determined directly from the excess energy at $x_{\text{Ni}} = 0.25, 0.5$, and 0.75 with no further optimisation.

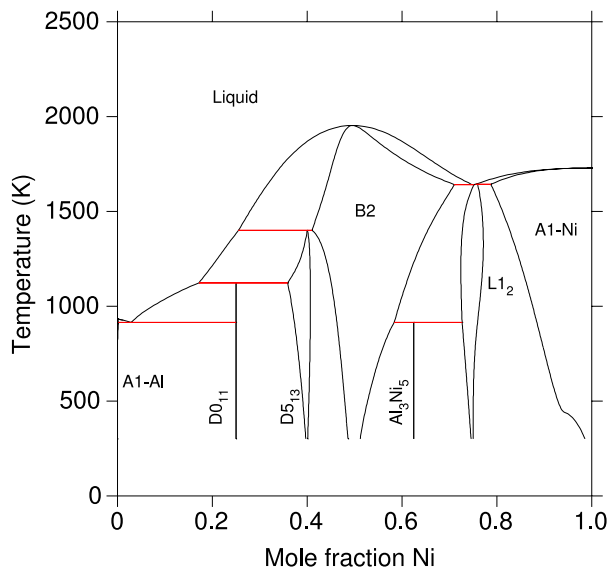


Fig. 6. The CALPHAD phase diagram from Dupin et al. [10], based on experimental and calculated thermodynamic and phase diagram data.

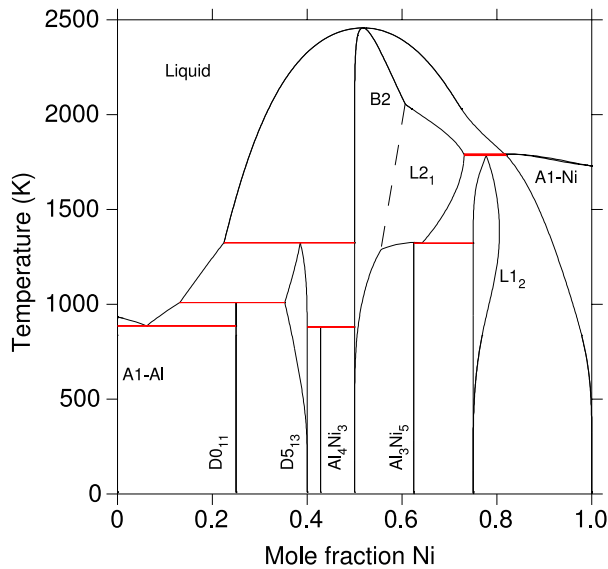


Fig. 7. The phase diagram obtained in this work, where the solid phase descriptions were obtained directly from first-principles calculation of thermodynamic properties, and the liquid description is taken directly from Dupin et al. [10].

using the same method may incur cancellation of errors while data from different calculation sources may be inherently incompatible. As such only data from the Debye-Grüneisen model describing the mixing of the disordered phases was used in the final tdb, with data from the phonon calculations at some compositions used for comparison.

The calculations of the Gibbs energy at various temperature and composition points were used to fit a Gibbs energy model as shown in equations (1) and (2). In order to minimise the impact of the offset between energies calculated using phonon calculations and the Debye-Grüneisen model, $G_m^{\text{dis}}(x_i)$ was initially considered using only data from the Debye-Grüneisen model, where $^{\circ}G_i$ is used directly and L_{ij}^{dis} are fitted. Then, the L_{ij}^{dis} were used in the database in combination with $^{\circ}G_i$ taken directly from the phonon calculations. There was reasonable agreement between the L_{ij}^{dis} parameters obtained using the fcc phonon calculations

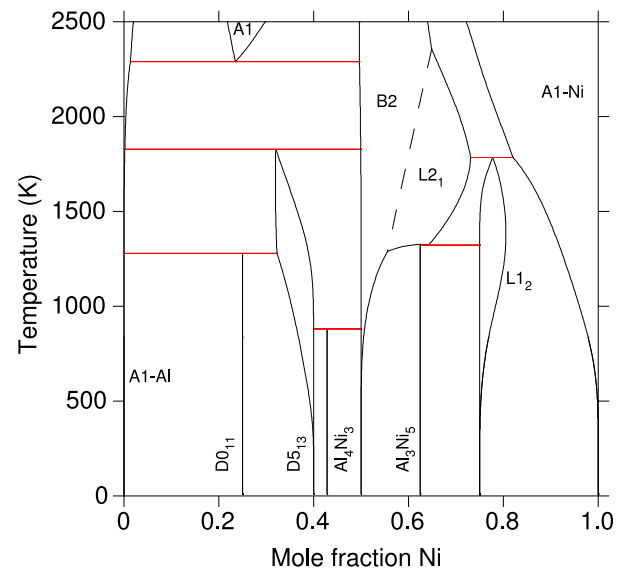


Fig. 8. Solid phase diagram obtained in this work using only first-principles data as input.

at various compositions and those obtained using the Debye-Grüneisen model at the same compositions.

Unlike the end-member phonon calculations that were fitted with a quadratic Gibbs energy function in temperature, it was found that a first order polynomial better reproduced the data calculated with the Debye-Grüneisen model, which were fitted between 0 K and 1500 K.

Fitting the disordered phase data to the temperature and composition parameterised model may be done in a variety of ways before being included in the database. Exact (direct) fitting of the excess energy of the disordered phase to the interaction parameters may be done but requires a large number of parameters and generally results in overfitting. Generally, such parameters are fitted as a compromise between the thermodynamic data relating to the disordered phase and the known phase boundaries. In this work, the calculated Gibbs energy as a function of temperature and composition was fitted directly to three intermediate compositions with a second order Redlich-Kister polynomial with coefficients given by low-order polynomials in temperature. This direct fitting is in contrast to the usual optimisation method where the phase boundaries are also considered in fitting the parameters of the phase. To correspond with the fitting of three intermediate compositions, the excess energy was considered using a Redlich-Kister polynomial of second order. To avoid overfitting of the data, the number of parameters used to describe the excess energy was kept as low as possible. The fitted disordered description for the fcc and bcc phases are shown compared to calculated data at several temperatures in Figs. 4 and 5 respectively.

For the disordered fcc solid solution phase, the interaction parameters were fitted giving priority to the Ni-rich data where the phase is stable. In Fig. 4 it can be seen that the calculated data do not exactly fit a smooth continuous curve at each temperature, and the calculated energies at $x_{\text{Ni}} = 0.5$ appears relatively too stable. These data are calculated from SQS, and the structure was fully relaxed during the DFT calculation. When using fully relaxed SQS calculations, the symmetry is naturally distorted from the ideal lattice because of size mismatch between atoms along with other factors [68]. This occurs to a different extent in each structure. In the $x_{\text{Ni}} = 0.5$ case, the energy stabilisation from full relaxation (compared to symmetry preserving volume relaxation) was greater than in other structures. Based on an analysis of the radial distribution function of relaxed and unrelaxed structures, it was found that while the other fcc structures had preserved symmetry during relaxation, the $x_{\text{Ni}} = 0.5$ has lost its fcc character. Therefore it is concluded that the $x_{\text{Ni}} = 0.5$ calculation is not a good representation of the fcc solid solution phase, and it is excluded from the fitting procedure.

For the disordered bcc solid solution phase, examination of the radial distribution function showed that the bcc symmetry was lost during full relaxation of the SQS. Therefore data was calculated using volume relaxation only, and compositions across the full composition range ($x_{\text{Ni}} = 0.25, 0.5, 0.75$) were used in the fitting to the Redlich-Kister polynomial.

The fitting of the disordered phase data has a significant effect on the phase boundaries in the resulting diagram. If, as is conventionally done, the experimental phase diagram data was simultaneously considered alongside the calculated Gibbs energy data, it would surely be possible to reasonably reproduce both the experimental phase boundaries and the calculated Gibbs energies. Optimisation considering experimental knowledge in this way may fit Gibbs energies that also include contributions that are not being considered in this work, such as the effects of short range ordering from higher order clusters beyond the pair approximation. However, in this work, only the calculated thermodynamic data for the phase being optimised in the BWG pair framework was considered.

5. Results and discussion

The phase diagram from the assessment by Dupin et al. [10] is shown in Fig. 6, and the phase diagram obtained using only first-principles data to describe the solid phases is shown in Fig. 7. All phase diagrams were calculated using the Thermo-Calc software package [69]. As no first-principles calculations were performed for the liquid phase, the liquid description from Dupin et al. is borrowed for comparison and used in this phase diagram. The assessed phase diagram from Dupin et al. [10] can be seen in Fig. 1 to reproduce the experimental phase diagram data well. All of the primary features of the experimentally-known phase diagram are reproduced by the phase diagram based on first-principles calculations in Fig. 7. The solid-only phase diagram is shown in Fig. 8 with the same temperature scale, however this cannot be compared with the equivalent metastable phase diagram from Dupin et al.'s experimentally based CALPHAD assessment as the high temperature extrapolations of the solid phases in the assessment from Dupin et al. are not well behaved.

The peritectic temperatures of the D0_{11} and D5_{13} phases are predicted with good agreement with experimental studies [11,12]. The CALPHAD phase diagram from Ansara et al. [9] (and also Dupin et al. [10]) has invariant reaction temperatures at 1123.6 K and 1410.3 K for the D0_{11} and D5_{13} phase respectively. This first-principles phase diagram in this work has the same reactions at 1008.8 K and 1324.7 K. The solubility of the D5_{13} phase is also predicted with good agreement with the experiment-based phase diagram. The Al_3Ni_5 phase is stable to a higher temperature than is experimentally observed and has a different invariant reaction type, but this is attributed to the modelling of the bcc phases with which it is in equilibrium. The fcc phases (A1 and L1_2) are present correctly, reproducing most of the topological features. The A1-Ni phase has solubility in agreement with experiment, and no solubility of the A1-Al phase is present. In the CALPHAD assessment from Dupin et al., following experimental investigation, the $\text{L1}_2\text{-AlNi}_3$ γ' phase does not melt congruently, but has an $\text{L1}_2 + \text{B2} \rightleftharpoons \text{liquid}$ eutectic reaction at 1642.2 K and 74.6 at.%Ni and an $\text{L1}_2 \rightleftharpoons \text{A1} + \text{liquid}$ peritectic reaction at 1643.3 K and 75.6 at.%Ni. Although these invariants are at approximately the correct temperature in the first-principles phase diagram (1783.2 K and 1790.8 K), the exact topology is not correctly predicted. This is attributed to the use of the liquid phase description from Dupin et al. that was optimised considering different solid descriptions. Furthermore, inaccuracies in the bcc and fcc phases may be attributed to the use of interaction parameters with temperature dependence obtained from the Debye-Grüneisen model in place of phonon calculations that have a higher-accuracy at these high temperatures.

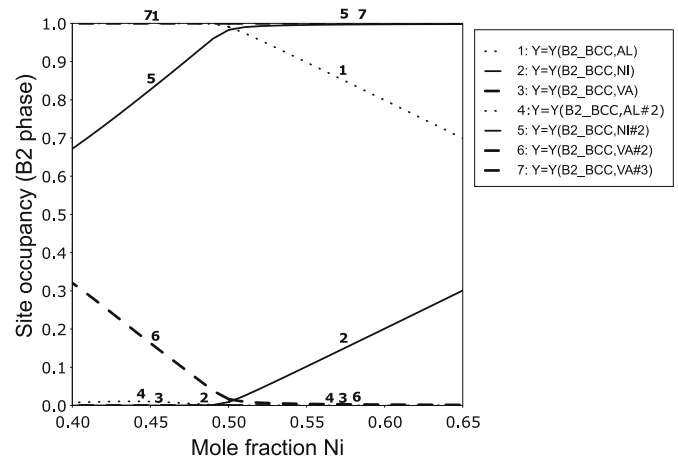


Fig. 9. Site occupancy of the B2 phase at 1500 K as modelled by Ansara et al. [9].

5.1. Liquidus

Comparing the experimentally-based and calculated phase diagrams in Figs. 6 and 7, it can be seen that the congruent melting temperature of the B2 phase relative to the liquid description from Ansara et al. and Dupin et al. [9,10] is higher than in the experimentally based phase diagram, at 2457 K compared to 1953 K. At first glance, this seems to suggest that the B2 Gibbs energy function derived from first-principles methods does not provide an adequate description. However, in the CALPHAD approach, in the absence of vast quantities of reliable experimental data pertaining to the liquid phase, the excess parameters describing the non-ideal mixing of liquid elements are often fitted considering experimentally known liquidus and solidus phase boundaries. Although neither Ansara et al. nor Dupin et al. give great detail of the process by which they arrived at the optimised parameters, by considering the available experimental information reported it is probable that the determination of the liquid parameters must have been done considering the known phase boundaries. This means that the liquid description is contingent on the solid phase descriptions from Ansara et al. or Dupin et al. to reproduce a physically correct phase diagram, rather than being independently determined. As the phase descriptions calculated from first-principles data in this work are not identical to the descriptions obtained via optimisation of parameters considering experimental data by Ansara et al. or Dupin et al., the same liquid description cannot be expected to produce a phase diagram with the same liquidus and solidus temperatures. While the description calculated in this work can only be used below the solidus, including the liquid phase from the assessed description from Dupin et al. as done in Fig. 7 can illustrate how significant the adjustments to the liquid parameters ought to be to obtain a description that reproduces the full condensed phase diagram.

5.2. Stability of L2_1 phase

In the phase diagram obtained from only first-principles data, the wide Ni-rich bcc solubility is present, but rather than being an extended B2 region as seen in the experimentally based CALPHAD phase diagram from Dupin et al. [10], there is a narrower B2 region and a second order phase boundary separating a binary L2_1 Heusler phase region further away from the ideal B2 stoichiometry (with sublattice condition $y_i^{(1)} = y_i^{(2)} \neq y_i^{(3)} \neq y_i^{(4)}$). This second order phase transition is marked approximately with a dashed line in the phase diagrams in Figs. 7 and 8. The bcc solubility is largely determined by the fitting of the disordered bcc phase. In this composition range, B2 and binary L2_1 are challenging to distinguish experimentally. As such, it is possible that the

experimentally determined B2 region was mischaracterised. However, the stability of the L2₁ phase could also be an artefact of the fitting procedure, or a result of the use of the Debye-Grüneisen model to obtain the temperature dependence of the Gibbs energy of the disordered phase. At 1500 K, the L2₁ phase is stable compared to the B2 phase by 1.5 kJ/mol at the Ni-rich solubility limit, with decreasing relative stability towards the B2/L2₁ phase boundary. This energy difference is within the uncertainty of the calculated data at this temperature, so conclusions cannot be drawn regarding the ordering behaviour, but the similarity of the energies of these two phases means that they can describe a representative phase diagram topology of an ordered bcc phase.

5.3. Al-rich B2 solubility

While the phase diagram produced in this work reproduces the general experimentally determined topology of the nickel-rich ordered bcc phases seen in the experimentally-based assessment from Dupin et al. in Fig. 6, it can clearly be seen in the calculated first-principles phase diagram in Fig. 7 that the B2 single phase region does not reproduce the experimentally seen aluminium-rich solubility of the B2 phase. In the phase diagram calculated in this work, where the description of the bcc phases comes only from first-principles calculations of ordered phases, there is very limited solubility on the Al-rich side.

As has been experimentally seen in the Al-Ni system [70] and has been modelled by Ansara et al. [9] (and then used by Dupin et al. [10]), the solubility of the B2 phase is facilitated by a different mechanism in the Al-rich and Ni-rich regions. In the work by Ansara et al., a three sublattice model (Al, Ni, Va)_{1/2}(Al, Ni, Va)_{1/2}(Va)₃ was used to model the B2 phase. The site occupancy for each constituent on each sublattice in the B2 phase at 1500 K, as modelled by Ansara et al., is shown in Fig. 9. In the Al-rich region, the solubility is primarily facilitated by vacancies on the second sublattice with almost no Al occupancy on that sublattice, while in the Ni-rich region, it is primarily facilitated by Al and Ni substitution on the first sublattice, with almost no vacancies present on either sublattice.

In this work, no vacancies were considered in the order-disorder partition model used for the bcc phases. The simplified model used correctly predicts that Al and Ni substitutions on each sublattice

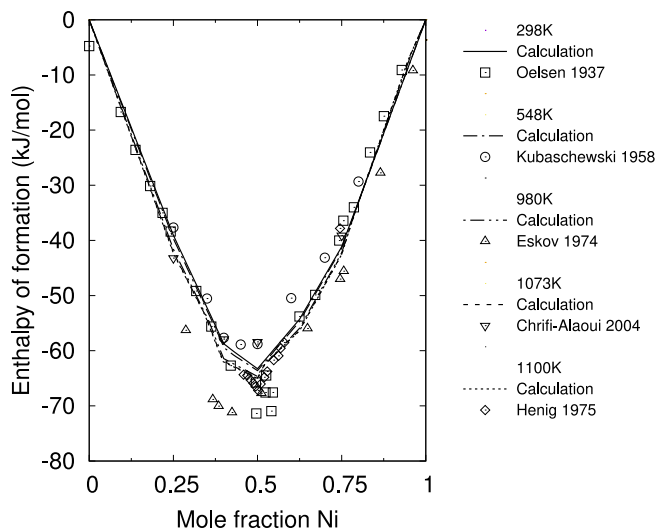


Fig. 10. Calculated enthalpy of formation of solid phases with respect to fcc Al and fcc Ni from this work at various temperatures (lines) compared with experimental measurements (points) [72–76].

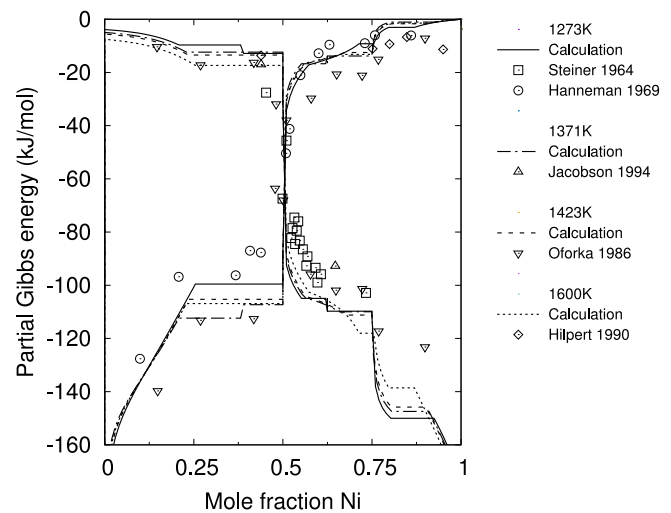


Fig. 11. Calculated partial molar Gibbs energy of aluminum and nickel with respect to fcc Al and fcc Ni at several temperatures (lines) compared with experimental measurements (points) [77–81].

facilitate the Ni-rich solubility, and that such substitutions do not produce a wide solubility region. However, without including vacancies in the sublattice model, there is no alternative mechanism to produce the desired Al-rich homogeneity range. As such, this solubility range cannot be expected to be reproduced in these calculations, and thus this feature is excluded from the comparison.

5.4. Magnetism

In the simplified model created in this work, the effects of magnetism were not directly considered with a magnetic term in the Gibbs energy expression. Pure nickel and nickel-rich compounds such as the γ' phase (AlNi₃-L1₂) are known to be magnetic, which is visible in a physical feature on the experiment-based phase diagram in Fig. 6 on the boundary between the Ni-rich L1₂ phase and Al-Ni. Without direct consideration of the contribution to the Gibbs energy due to magnetism via specific physical models, such feature is very difficult to reproduce. In the first-principles calculations used in this work, spin polarisation was used for magnetic phases, so that the magnetism of the end-member phases was treated implicitly. However, it can be seen that the variation of the magnetic contribution with composition is not as experimentally observed, and the L1₂-Al boundary in this first-principles only phase diagram in Fig. 7 is smooth and continuous.

5.5. Stability of Al₄Ni₃

The ambiguity regarding the Al₄Ni₃ phase has led to its exclusion from some phase diagrams. In the calculated phase diagram in this work, the Al₄Ni₃ phase appears as a stable phase from the ground state up to 880 K. This is consistent with the experimental investigations regarding this phase [7] and the transition temperature of 853 K in the experimental phase diagram from Urrutia et al. [8]. The Al₄Ni₃ phase appears in competition with the D5₁₃ phase and the ordered B2 phase. While the Al₄Ni₃ phase appears on the Al-Ni convex hull at low temperature, as shown in Fig. 2, because the substoichiometric extension of the B2 phase due to vacancies is not modelled in this work, this cannot be said to conclusively demonstrate the prediction that the Al₄Ni₃ phase is stable at higher temperatures. However, considering the experimentally observed solubility of the B2 phase, it would not be expected to fully destabilise any precipitation of the Al₄Ni₃ phase.

5.6. Thermodynamic properties

As well as considering the topology of the phase diagram, a comparison with the experimental thermodynamic data may also be made. Fig. 10 shows the calculated heat content from this work at various temperatures compared with experimental measurements. It can be seen that the experimental data is reproduced within the range of scatter. The aluminum-rich side is better reproduced by the calculations in this work than by the assessment from Ansara et al. [9]. This was similarly seen in an assessment of the Al-Ni phase diagram by Chen et al. [71] incorporating first-principles insights.

Fig. 11 shows the partial Gibbs energy of aluminum and nickel calculated in this work compared with experimental measurements at various temperatures. Within this temperature range, the liquid phase is present at some compositions, so only a rough comparison can be made using the borrowed liquid description that is not optimised considering the solid phases. Despite this, it can be seen that the experimental data is reproduced reasonably within the scatter, with a similar degree of agreement to the assessment from Ansara et al. [9]. The major discrepancies concern the B2 phase, where the aluminum-rich side was not modelled in this work.

6. Conclusions

In recent years, the use of first-principles calculations in CALPHAD assessments has become standard practice, but complex features and disordered phases have generally meant that first-principles calculations alone have not been able to fully substitute all experimental data when used in the conventional way. This work attempts to harness various sublattice modelling and cluster approximation techniques to fully parameterise a thermodynamic description of the solid phases in the aluminium-nickel system directly from first-principles calculations of the Gibbs energy.

DFT and phonon calculations were performed for ordered phases, and SQS were used alongside the Debye-Grüneisen model to consider the disordered phases. Four substitutional sublattice order-disorder partitioning models were used together with the Bragg-Williams-Gorsky model to include an energy contribution that mimics the effect of short range ordering. The Gibbs energy functions were obtained entirely through direct fitting to the calculated first-principles single phase data, without considering any experimental thermodynamic or phase diagram information. The liquid phase was not modelled in this work, and so the liquid description was borrowed from the widely-used assessment from Dupin et al. [10]. The resulting phase diagram predicts all major features such as the stable phases and ranges of solubility of the experimentally known phase diagram.

As the liquid description was optimised considering a different set of solid phase Gibbs energy functions by Dupin et al., the liquidus is not fully reproduced, however, its topological similarity indicates good agreement between the previously assessed Gibbs energies and the ones

calculated in this work. Unlike the assessment from Dupin et al., the first-principles phase diagram predicts the stability of an Al_4Ni_3 phase that has been intermittently experimentally observed but generally not considered as one of the stable phases in this system. The first-principles phase diagram also predicts that the wide Ni-rich solubility of the ordered bcc phase has a second order phase transition from B2 to L_{21} far from the B2 stoichiometry, which may give some insight into the bcc ordering. Vacancies were not considered as a constituent in the bcc phases therefore no Al-rich solubility is present. No specific magnetic features were considered in this work.

Using the aluminium-nickel system as a prototype, this work demonstrates that it is possible to obtain a CALPHAD phase diagram for a solid system at a practical application level using only first-principles calculations as input, that may be used both to consider unknown systems and for materials informatics explorations. Such a diagram could be used alongside preliminary experimental investigations to guide future experiments, potentially saving significant time and expense.

Funding

This work was supported in part by Ministry of Education, Culture, Sports, Science and Technology (MEXT) of Japan as a social and scientific priority issue (Creation of new functional devices and high-performance materials to support next-generation industries; CDMSI) to be tackled by using post-K computer.

Data availability

The raw data required to reproduce these findings cannot be shared at this time as the data also forms part of an ongoing study. The processed data required to reproduce the original phase diagram calculations is available in the tdb file provided in the supplementary files. The remaining processed data required to reproduce these findings cannot be shared at this time as the data also forms part of an ongoing study.

Declaration of competing interest

The authors declare that they have no known competing financial interests or personal relationships that could have appeared to influence the work reported in this paper.

Acknowledgements

The authors acknowledge the Center for Computational Materials Science of the Institute for Materials Research, Tohoku University, for the support of the supercomputing facilities.

The authors would like to thank Nathalie Dupin and Suzana G. Fries for helpful discussion in the early stages of this work. TD would like to thank Bonnie Hagen (previously Lindahl) for her tireless assistance with the bcc order-disorder model.

Appendix A

Four-sublattice construction for the fcc phases

As described by Kusoffsky et al., each of the four sublattices is a cubic sublattice of the fcc cell, which form four corners of a tetrahedron in the unit cell. This is shown in Fig. 12. By the crystallographic symmetry of the fcc lattice, each site on the tetrahedron must be equivalent, and the bond length between each atom in the tetrahedron must be equal and of first nearest neighbour (1nn) type. The next nearest neighbour (2nn) for each atom is its equivalent site on the next tetrahedron. In Fig. 12, some of the 1nn bonds are indicated with dashed lines, and some 2nn bonds are shown with solid lines. Each sublattice is equivalent and therefore contains a quarter of the atoms per mole. Therefore, the four-sublattice model used to describe the various ordered fcc-based structures is $(\text{Al}, \text{Ni})_{1/4}(\text{Al}, \text{Ni})_{1/4}(\text{Al}, \text{Ni})_{1/4}(\text{Al}, \text{Ni})_{1/4}$.

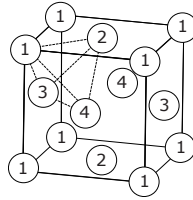


Fig. 12. The fcc crystal structure indicating the sites of the four symmetrically equivalent sublattices. 1nn bonds are shown with dashed lines, and 2nn bonds with solid lines.

The four-sublattice model has the possible sublattice occupation ordered end-members (where each sublattice is singularly occupied) fcc-Al (A1), Al₃Ni (L1₂), AlNi (L1₀), AlNi₃ (L1₂), and fcc-Ni (A1). The energy of each fully ordered compound with respect to the pure elements in the disordered state is considered in terms of the unlike 1nn bond energy by counting the number of equivalent 1nn bonds in each structure.

Four-sublattice construction for the bcc phases

A similar tetrahedron construction was used by Abe and Shimono [34] to represent the bcc phases, but while fcc phases have a single lattice parameter defining the volume, the asymmetry of the *a* and *c* lattice parameter in the conventional bcc unit cell means that the six bonds within the tetrahedron are of either 1nn and 2nn type, and the bonds between equivalent sites on neighbouring tetrahedra are of third nearest neighbour (3nn) type.

Fig. 13 Shows an example of the 1nn and 2nn bonds in the bcc unit cell.

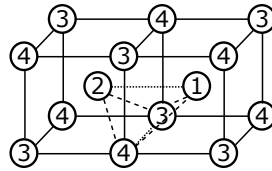


Fig. 13. The bcc crystal structure, indicating the sites of the four sublattices. The four sublattice sites make a repeating tetrahedron structure. The 1nn bonds in the tetrahedron are marked with dashed lines, and the 2nn bonds are marked with dotted lines. The solid lines mark the cubic cell, and do not correspond to the 3nn bonds.

The crystal structure may be separated into two pairs of equivalent sublattices, each containing a quarter of the atoms. The four sublattice model is therefore (Al, Ni)_{1/4}(Al, Ni)_{1/4}(Al, Ni)_{1/4}(Al, Ni)_{1/4}. The presence of 1nn and 2nn bonds within the tetrahedron construction arising from the asymmetry of the bcc sublattice results in two different possible ordering configurations in an equiatomic binary compound. The end-member ordered phases for the bcc four-sublattice model are therefore Al (A2), Al₃Ni (D0₃), AlNi (B2), AlNi (B32), AlNi₃ (D0₃), and Ni (A2).

Following Abe and Shimono [34] and Lindahl et al. [36], a pair interaction model is constructed to relate the reciprocal interaction parameters to the energies of the end-member compounds within a four substitutional sublattice order-disorder partitioning model. It is again assumed that all ordering energy in the compound relative to the end-members comes from the unlike bonds. From Lindahl et al., the number of bonds may be averaged over the number of tetrahedra that share the bond, so as to avoid double counting any bonds [36]. Each 1nn bond is shared by six tetrahedra, each 2nn bond is shared by four tetrahedra, and each tetrahedron contains four atoms shared between 24 tetrahedra. Therefore the Gibbs energy of each of the end-members *ijkl* for the above model, $G_{ijkl}^{\text{bcc-ord}(4\text{SL})}$, can be expressed in terms of the number of 1nn bonds, *x*, and 2nn bonds, *y* as

$$G_{ijkl}^{\text{bcc-ord}(4\text{SL})} = \frac{\frac{x}{6}u_{AB}^{\text{bcc}} + \frac{y}{4}v_{AB}^{\text{bcc}}}{\frac{4}{24}} = x \cdot u_{AB}^{\text{bcc}} + \frac{3}{2}y \cdot v_{AB}^{\text{bcc}} \quad (46)$$

where u_{AB}^{bcc} and v_{AB}^{bcc} are the 1nn and 2nn bond energy respectively.

Appendix B. Supplementary data

Supplementary data to this article can be found online at <https://doi.org/10.1016/j.calphad.2020.102008>.

References

- [1] R. Nazarov, T. Hickel, J. Neugebauer, Vacancy formation energies in fcc metals: influence of exchange-correlation functionals and correction schemes, *Phys. Rev. B* 85 (14) (2012) 1–7, <https://doi.org/10.1103/PhysRevB.85.144118>.
- [2] Materials Genome Initiative for Global Competitiveness. <https://www.mgi.gov/>, 2011.
- [3] A.I. Duff, T. Davey, D. Korbmaier, A. Glensk, B. Grabowski, J. Neugebauer, M. W. Finnis, An improved method of calculating ab initio high-temperature thermodynamic properties with application to ZrC, *Phys. Rev. B* 91 (2015) 214311, <https://doi.org/10.1103/PhysRevB.91.214311>.
- [4] L.F. Zhu, B. Grabowski, J. Neugebauer, Efficient approach to compute melting properties fully from ab initio with application to Cu, *Phys. Rev. B* 96 (22) (2017), <https://doi.org/10.1103/PhysRevB.96.224202>.
- [5] Z.-K. Liu, First-principles calculations and CALPHAD modeling of thermodynamics, *J. Phase Equilibria Diffus.* 30 (5) (2009) 517–534, <https://doi.org/10.1007/s11669-009-9570-6>.
- [6] M. Palumbo, S.G. Fries, T. Hammerschmidt, T. Abe, J.C. Crivello, A.A.H. Breidi, J. M. Joubert, R. Drautz, First-principles-based phase diagrams and thermodynamic properties of TCP phases in Re-X systems (X = Ta, V, W), *Comput. Mater. Sci.* 81 (2014) 433–445, <https://doi.org/10.1016/j.commatsci.2013.08.051>.
- [7] M. Ellner, S. Kek, B. Predel, Ni₃Al₄ - a phase with ordered vacancies isotypic to Ni₃Ga₄, *J. Less Common Met.* 154 (1989) 207–215, [https://doi.org/10.1016/0022-5088\(89\)90185-9](https://doi.org/10.1016/0022-5088(89)90185-9).
- [8] A. Urrutia, S. Tumminello, S.F. Arico, S. Sommadossi, Characterization of Al – Ni intermetallics around 30 – 60 at % Al for TLPB application, *Calphad* 44 (2014) 108–113, <https://doi.org/10.1016/j.calphad.2013.08.004>.
- [9] I. Ansara, N. Dupin, H.L. Lukas, B. Sundman, Thermodynamic assessment of the Al-Ni system, *J. Alloys Compd.* 247 (1997) 20–30, [https://doi.org/10.1016/S0925-8388\(96\)02652-7](https://doi.org/10.1016/S0925-8388(96)02652-7).

- [10] N. Dupin, I. Ansara, B. Sundman, Thermodynamic re-assessment of the ternary system Al-Cr-Ni, *Calphad* 25 (2) (2001) 279–298, [https://doi.org/10.1016/S0364-5916\(01\)00049-9](https://doi.org/10.1016/S0364-5916(01)00049-9).
- [11] A.G.C. Gwyer, Alloys of aluminum with copper, iron, nickel, cobalt, lead and cadmium, *Z. Anorg. Chem.* 57 (1908) 113–153, <https://doi.org/10.1002/zaac.19080570106>.
- [12] W.O. Alexander, N.B. Vaughan, Investigation of phase equilibria in Al-Ni system, *J. Inst. Met.* 61 (1937) 247–260.
- [13] J. Schramm, *Z. Metallkd.* 33 (1941) 327.
- [14] A. Taylor, R.W. Floyd, The constitution of nickel-rich alloys of the nickel chromium titanium system, *J. Inst. Met.* 80 (11) (1952) 577.
- [15] A. Taylor, N.J. Doyle, Further studies on the nickel-aluminum system. I. The beta-NiAl and delta-Ni₂Al₃ phase fields, *J. Appl. Crystallogr.* 5 (1972) 201, <https://doi.org/10.1107/S0021889872009203>.
- [16] P. Nash, D.R.F. West, Ni-Al and Ni-Ta phase diagrams, *Met. Sci.* 17 (2) (1983) 99–100, <https://doi.org/10.1179/030634583790427649>.
- [17] I.M. Robertson, C.M. Wayman, Ni₅Al₃ and the nickel-aluminum binary phase diagram, *Metallography* 17 (1984) 43–55, [https://doi.org/10.1016/0026-0800\(84\)90004-1](https://doi.org/10.1016/0026-0800(84)90004-1).
- [18] K. Hilpert, D. Kobertz, V. Venugopal, M. Miller, H. Gerads, F.J. Bremer, H. Nickel, Phase diagram studies on the Al-Ni system, *Z. Naturforsch.* 42a (1987) 1327–1332, <https://doi.org/10.1515/zna-1987-1117>.
- [19] F.J. Bremer, M. Beyss, E. Karthaus, A. Hellwig, T. Schöber, J.-M. Welter, H. Wenzl, Experimental analysis of the Ni-Al phase diagram, *J. Cryst. Growth* 87 (1988) 185–192, [https://doi.org/10.1016/0022-0248\(88\)90163-7](https://doi.org/10.1016/0022-0248(88)90163-7).
- [20] R. D. Noebe, Unpublished results (1991).
- [21] R.D. Noebe, R.R. Bowman, M.V. Nathal, Physical and mechanical properties of the B2 compound NiAl, *Int. Mater. Rev.* 38 (4) (1993) 193, <https://doi.org/10.1179/imr.1993.38.4.193>.
- [22] J.D. Verhoeven, J.H. Lee, F.C. Laabs, L.L. Jones, The phase equilibria of Ni₃Al evaluated by directional solidification and diffusion couple experiments, *J. Phase Equil.* 12 (1) (1991) 15–23, <https://doi.org/10.1007/BF02663666>.
- [23] A.L. Udovskii, V.G. Moldavskii, V.Z. Turkevich, Revision of phase diagram of nickel-aluminum system, *Dokl. Phys. Chem.* 317 (1) (1991) 234–237.
- [24] A.L. Udovskii, I.V. Oldakovskii, V.G. Moldavskii, Theoretical and experimental study of phase equilibrium in the Ni-NiAl-W system over the temperature range 900–1500 Deg C, *Russ. Metall.* 4 (1991) 111–122.
- [25] J.G. Goiri, A. Van der Ven, Phase and structural stability in Ni-Al systems from first principles, *Phys. Rev. B* 94 (9) (2016), 094111, <https://doi.org/10.1103/PhysRevB.94.094111>.
- [26] A. van de Walle, R. Sun, Q.-j. Hong, S. Kadkhodaei, Software tools for high-throughput CALPHAD from first-principles data, *Calphad* 58 (March) (2017) 70–81, <https://doi.org/10.1016/j.calphad.2017.05.005>.
- [27] S. Bhattacharya, R. Sahara, K. Ohno, A first-principles phase field method for quantitatively predicting multi-composition phase separation without thermodynamic empirical parameter, *Nat. Commun.* 10 (1) (2019) 3451, <https://doi.org/10.1038/s41467-019-11248-z>.
- [28] A. Pasturel, C. Colinet, A.T. Paxton, M.V. Schilfgaard, First-principles determination of the Ni-Al phase diagram, *J. Phys. Condens. Matter* 4 (1999) 945–959, <https://doi.org/10.1088/0953-8984/4/4/005>.
- [29] W.L. Bragg, E.J. Williams, The effect of thermal agitation on atomic arrangement in alloys, *Proc. Roy. Soc.* 145 (855) (1934) 699–730, <https://doi.org/10.1098/rspa.1934.0132>.
- [30] T. Mohri, J.M. Sanchez, D. de Fontaine, Overview No. 43: binary ordering prototype phase diagrams in the cluster variation approximation, *Acta Metall.* 33 (7) (1985) 1171–1185, [https://doi.org/10.1016/0001-6160\(85\)90228-7](https://doi.org/10.1016/0001-6160(85)90228-7).
- [31] R. Kikuchi, A theory of cooperative phenomena, *Phys. Rev.* 81 (6) (1951) 988–1003, <https://doi.org/10.1103/PhysRev.81.988>.
- [32] A. Kusoffsky, N. Dupin, B. Sundman, On the compound energy formalism applied to fcc ordering, *Calphad* 25 (4) (2001) 549–565, [https://doi.org/10.1016/S0364-5916\(02\)00007-X](https://doi.org/10.1016/S0364-5916(02)00007-X).
- [33] W. Gorsky, Röntgenographische untersuchung von Umwandlungen in der Legierung CuAu, *Z. Phys.* 50 (1–2) (1928) 64–81, <https://doi.org/10.1007/BF01328593>.
- [34] T. Abe, M. Shimono, A description of the effect of short-range ordering in BCC phases with four sublattices, *Calphad* 45 (2014) 40–48, <https://doi.org/10.1016/j.calphad.2013.11.006>.
- [35] B. Sundman, S.G. Fries, W.A. Oates, A thermodynamic assessment of the Au-Cu system, *Calphad* 22 (3) (1998) 335–354, [https://doi.org/10.1016/S0364-5916\(98\)00034-0](https://doi.org/10.1016/S0364-5916(98)00034-0).
- [36] B.B. Lindahl, B.P. Burton, M. Selleby, Ordering in ternary BCC alloys applied to the Al-Fe-Mn system, *Calphad* 51 (2015) 211–219, <https://doi.org/10.1016/j.calphad.2015.09.008>.
- [37] C. Wagner, W. Schottky, Theory of regular mixed phases, *Z. Phys. Chem.* 11 (1930) 163–210.
- [38] A. Zunger, S.-H. Wei, L.G. Ferreira, J.E. Bernard, Special quasirandom structures, *Phys. Rev. Lett.* 65 (3) (1990) 353–356, <https://doi.org/10.1103/PhysRevLett.65.353>.
- [39] A. van de Walle, P. Tiwary, M. De Jong, D.L. Olmsted, M. Asta, A. Dick, D. Shin, Y. Wang, L.-Q. Chen, Z.-K. Liu, Efficient stochastic generation of special quasirandom structures, *Calphad* 42 (2013) 13–18, <https://doi.org/10.1016/j.calphad.2013.06.006>.
- [40] C. Wolverton, Crystal structure and stability of complex precipitate phases in Al-Cu-Mg-(Si) and Al-Zn-Mg alloys, *Acta Mater.* 49 (16) (2001) 3129–3142, [https://doi.org/10.1016/S1359-6454\(01\)00229-4](https://doi.org/10.1016/S1359-6454(01)00229-4).
- [41] C. Jiang, C. Wolverton, J. Sofo, L.-Q. Chen, Z.-K. Liu, First-principles study of binary bcc alloys using special quasirandom structures, *Phys. Rev. B* 69 (21) (2004) 214202, <https://doi.org/10.1103/PhysRevB.69.214202>.
- [42] G. Kresse, D. Joubert, From ultrasoft pseudopotentials to the projector augmented-wave method, *Phys. Rev. B* 59 (3) (1999) 1758–1775, <https://doi.org/10.1103/PhysRevB.59.1758>.
- [43] G. Kresse, J. Hafner, Ab initio molecular-dynamics simulation of the liquid-metal-amorphous-semiconductor transition in germanium, *Phys. Rev. B* 49 (20) (1994) 14251–14269, <https://doi.org/10.1103/PhysRevB.49.14251>.
- [44] G. Kresse, J. Furthmüller, Efficiency of ab-initio total energy calculations for metals and semiconductors using a plane-wave basis set, *Comput. Mater. Sci.* 6 (1) (1996) 15–50, [https://doi.org/10.1016/0927-0256\(96\)00008-0](https://doi.org/10.1016/0927-0256(96)00008-0).
- [45] G. Kresse, J. Furthmüller, Efficient iterative schemes for ab initio total-energy calculations using a plane-wave basis set, *Phys. Rev. B* 54 (16) (1996) 11169–11186, <https://doi.org/10.1103/PhysRevB.54.11169>.
- [46] J.P. Perdew, K. Burke, M. Ernzerhof, Generalized gradient approximation made simple, *Phys. Rev. Lett.* 77 (18) (1996) 3865, <https://doi.org/10.1103/PhysRevLett.77.3865>.
- [47] J.P. Perdew, K. Burke, M. Ernzerhof, Generalized gradient approximation made simple- ERRATA, *Phys. Rev. Lett.* 78 (7) (1996) 1396, <https://doi.org/10.1103/PhysRevLett.78.1396>.
- [48] H.J. Monkhorst, J.D. Pack, Special points for Brillouin-zone integrations, *Phys. Rev. B* 13 (12) (1976) 5188–5192, <https://doi.org/10.1103/PhysRevB.13.5188>.
- [49] Y. Wang, Z.-K. Liu, L.-Q. Chen, Thermodynamic properties of Al, Ni, NiAl, and Ni₃Al from first-principles calculations, *Acta Mater.* 52 (9) (2004) 2665–2671, <https://doi.org/10.1016/j.actamat.2004.02.014>.
- [50] R. Arroyave, D. Shin, Z.-K. Liu, Ab initio thermodynamic properties of stoichiometric phases in the Ni-Al system, *Acta Mater.* 53 (6) (2005) 1809–1819, <https://doi.org/10.1016/j.actamat.2004.12.030>.
- [51] A. van de Walle, M. Asta, G. Ceder, The alloy theoretic automated toolkit: a user guide, *Calphad* 26 (4) (2002) 539–553, [https://doi.org/10.1016/S0364-5916\(02\)80006-2](https://doi.org/10.1016/S0364-5916(02)80006-2).
- [52] A.C. Lieser, C.L. Zacherl, A. Saengdeejing, Z.-K. Liu, L.J. Kecskes, First-principles calculations and thermodynamic re-modeling of the Hf-W system, *Calphad* 38 (2012) 92–99, <https://doi.org/10.1016/j.calphad.2012.04.005>.
- [53] X.L. Liu, C.Z. Hargather, Z.-K. Liu, First-principles aided thermodynamic modeling of the Nb-Re system, *Calphad* 41 (2013) 119–127, <https://doi.org/10.1016/j.calphad.2013.02.006>.
- [54] S.L. Shang, Y. Wang, D. Kim, Z.-K. Liu, First-principles thermodynamics from phonon and Debye model: application to Ni and Ni₃Al, *Comput. Mater. Sci.* 47 (2010) 1040–1048, <https://doi.org/10.1016/j.commatsci.2009.12.006>.
- [55] V.L. Moruzzi, J.F. Janak, K. Schwarz, Calculated thermal properties of metals, *Phys. Rev. B* 37 (2) (1988) 790–799, <https://doi.org/10.1103/PhysRevB.37.790>.
- [56] N. Saunders, A.P. Miodownik, A.T. Dinsdale, Metastable lattice stabilities for the elements, *Calphad* 12 (4) (1988) 351–374, [https://doi.org/10.1016/0364-5916\(88\)90038-7](https://doi.org/10.1016/0364-5916(88)90038-7).
- [57] Y. Wang, S. Curtarolo, C. Jiang, R. Arroyave, T. Wang, G. Ceder, L.-Q. Chen, Z.-K. Liu, Ab initio lattice stability in comparison with CALPHAD lattice stability, *Calphad* 28 (1) (2004) 79–90, <https://doi.org/10.1016/j.calphad.2004.05.002>.
- [58] A. van de Walle, Reconciling SGTE and ab initio enthalpies of the elements, *Calphad* 60 (September 2017) (2018) 1–6, <https://doi.org/10.1016/j.calphad.2017.10.008>.
- [59] A. van de Walle, Q. Hong, S. Kadkhodaei, R. Sun, The free energy of mechanically unstable phases, *Nat. Commun.* 6 (May) (2015) 7559, <https://doi.org/10.1038/ncomms8559>.
- [60] M. Mantina, Y. Wang, L.Q. Chen, Z.K. Liu, C. Wolverton, First principles impurity diffusion coefficients, *Acta Mater.* 57 (14) (2009) 4102–4108, <https://doi.org/10.1016/j.actamat.2009.05.006>.
- [61] M. Mantina, Y. Wang, R. Arroyave, S.L. Shang, L.Q. Chen, Z.K. Liu, A first-principles approach to transition states of diffusion, *J. Phys. Condens. Matter* 24 (30) (2012) 305402, <https://doi.org/10.1088/0953-8984/24/30/305402>.
- [62] B. Sundman, F. Aldinger, The Ringberg workshop 1995 on unary data for elements and other end-members of solutions, *Calphad* 19 (4) (1995) 433–436, [https://doi.org/10.1016/0364-5916\(96\)00001-6](https://doi.org/10.1016/0364-5916(96)00001-6).
- [63] A.T. Dinsdale, SGTE data for pure elements, *Calphad* 15 (4) (1991) 317–425, [https://doi.org/10.1016/0364-5916\(91\)90030-N](https://doi.org/10.1016/0364-5916(91)90030-N).
- [64] Q. Chen, B. Sundman, Modeling of thermodynamic properties for bcc, fcc, liquid, and amorphous iron, *J. Phase Equil.* 22 (6) (2001) 631–644, <https://doi.org/10.1007/s11669-001-0027-9>.
- [65] I. Roslyakova, B. Sundman, H. Dette, L. Zhang, I. Steinbach, Modeling of Gibbs energies of pure elements down to 0 K using segmented regression, *Calphad* 55 (2016) 165–180, <https://doi.org/10.1016/j.calphad.2016.09.001>.
- [66] A. Dinsdale, O. Zobac, A. Kroupa, A. Khvan, Use of third generation data for the elements to model the thermodynamics of binary alloy systems: Part 1 – the critical assessment of data for the Al-Zn system, *Calphad* 68 (2020) 101723, <https://doi.org/10.1016/j.calphad.2019.101723>.
- [67] A. Van de Walle, G. Ceder, U.V. Waghmare, First-principles computation of the vibrational entropy of ordered and disordered Ni₃Al, *Phys. Rev. Lett.* 80 (22) (1998) 4911–4914, <https://doi.org/10.1103/PhysRevLett.80.4911>.
- [68] D. Shin, R. Arroyave, Z.-K. Liu, Thermodynamic properties of binary hcp solution phases from special quasirandom structures, *Phys. Rev. B* 74 (2006), 024204, <https://doi.org/10.1103/PhysRevB.74.024204>.
- [69] J.-O. Andersson, T. Helander, L. Hoglund, P. Shi, B. Sundman, THERMO-CALC & DICTRA, computational tools for materials science, *Calphad* 26 (2) (2002) 273–312, [https://doi.org/10.1016/S0364-5916\(02\)00037-8](https://doi.org/10.1016/S0364-5916(02)00037-8).

- [70] A.J. Bradley, A. Taylor, An X-ray analysis of the nickel-aluminium system, *Proc. R. Soc.* 159 (896) (1937) 56–72, <https://doi.org/10.1098/rspa.1937.0056>.
- [71] H.L. Chen, E. Doernberg, P. Svoboda, R. Schmid-fetzer, Thermodynamics of the Al₃Ni phase and revision of the Al-Ni system, *Thermochim. Acta* 512 (1–2) (2011) 189–195, <https://doi.org/10.1016/j.tca.2010.10.005>.
- [72] W. Oelsen, W. Middel, The thermochemistry of alloys. I." direct determination of the heats of formation of the alloy series cobalt-silicon, iron-aluminum, cobalt-aluminum, nickel-aluminum, copper-aluminum and antimony-zinc for the cast state, *Mitt. Kaiser Wilhelm Inst. Eisenforsch* 19 (1937) 1–26.
- [73] O. Kubaschewski, The heats of formation in the system aluminium + nickel + titanium, *Trans. Faraday Soc.* 54 (1958) 814–820, <https://doi.org/10.1039/TF9585400814>.
- [74] V.M. Es'kov, V.V. Samokhval, A.A. Vecher, *Russ. Metall.* 2 (1974) 118.
- [75] F.Z. Chrifi-Alaoui, M. Nassik, K. Mahdouk, J.C. Gachon, Enthalpies of formation of the Al – Ni intermetallic compounds . Enthalpies of formation of the Al – Ni intermetallic compounds, *J. Alloys Compd.* 364 (2004) 121–126, [https://doi.org/10.1016/S0925-8388\(03\)00493-6](https://doi.org/10.1016/S0925-8388(03)00493-6).
- [76] E.T. Henig, H.L. Lukas, Kalorimetrische Bestimmung der Bildungsenthalpie und die Beschreibung der Fehlordnung der Geordneten-Phase (Ni, Cu)_{1-x}Al_x, *Z. Metallkd.* 66 (1975) 98.
- [77] A. Steiner, K.L. Komarek, Thermodynamic activities of solid nickel-aluminum alloys, *Trans. Metall. Soc. AIME* 230 (4) (1964) 786.
- [78] R.E. Hanneman, A.U. Seybolt, Nickel activity data in the nickel-aluminum system at 1000°C, *Trans. Metall. Soc. AIME* 245 (2) (1969) 434–435.
- [79] N.S. Jacobson, Applications of thermodynamics in the synthesis and processing of materials: proceedings of a symposium, in: B.S. P Nash (Ed.), *Applications of Thermodynamics in the Synthesis and Processing of Materials*, TMS, 1994.
- [80] N.C. Oforka, Thermodynamics of aluminium-nickel alloys, *Indian J. Chem.* 25A (November) (1986) 1027–1029.
- [81] K. Hilpert, M. Miller, H. Gerads, H. Nickel, Thermodynamic study of the liquid and solid alloys of the nickel-rich part of the Al-Ni phase diagram including the AlNi₃ phase, *Ber. Bunsen Ges. Phys. Chem.* 94 (1990) 40–47, <https://doi.org/10.1002/bbpc.19900940109>.